

Effects of dust evolution on the abundances of CO and H₂

Hiroyuki Hirashita^{1*} and Nanase Harada¹

¹*Institute of Astronomy and Astrophysics, Academia Sinica, PO Box 23-141, Taipei 10617, Taiwan*

Accepted XXX. Received YYY; in original form ZZZ

ABSTRACT

The CO-to-H₂ conversion factor (X_{CO}) is known to correlate with the metallicity (Z). The dust abundance, which is related to the metallicity, is responsible for this correlation through dust shielding of dissociating photons and H₂ formation on dust surfaces. In this paper, we investigate how the relation between dust-to-gas ratio and metallicity (\mathcal{D} - Z relation) affects the H₂ and CO abundances (and X_{CO}) of a ‘molecular’ cloud. For the \mathcal{D} - Z relation, we adopt a dust evolution model developed in our previous work, which treats the evolution of not only dust abundance but also grain sizes in a galaxy. Shielding of dissociating photons and H₂ formation on dust are solved consistently with the dust abundance and grain sizes. As a consequence, our models predict consistent metallicity dependence of X_{CO} with observational data. Among various processes driving dust evolution, grain growth by accretion has the largest impact on the X_{CO} - Z relation. The other processes also have some impacts on the X_{CO} - Z relation, but their effects are minor compared with the scatter of the observational data at the metallicity range ($Z \gtrsim 0.1 Z_{\odot}$) where CO could be detected. We also find that dust condensation in stellar ejecta has a dramatic impact on the H₂ abundance at low metallicities ($\lesssim 0.1 Z_{\odot}$), relevant for damped Lyman α systems and nearby dwarf galaxies, and that the grain size dependence of H₂ formation rate is also important.

Key words: methods: analytical — molecular processes — dust, extinction — galaxies: evolution — galaxies: ISM — radio lines: galaxies

1 INTRODUCTION

Galaxies evolve through star formation. Since molecular clouds are the birth place of stars, understanding how molecular clouds evolve provides us with an important key to how stars form in galaxies. The main chemical constituent of molecular clouds is molecular hydrogen (H₂). Since emission from H₂ is weak in cold molecular environments (H₂ emission is more easily observed in regions with shock or ultraviolet excitation; e.g. Naslim et al. 2015 for a recent observation), emission from carbon monoxide (CO) is often used as a tracer of molecular clouds. Thus, understanding the formation and evolution of H₂ and CO and the relation between these two species is important to clarify to what extent CO can really trace molecular clouds at various stages of galaxy evolution.

In the present Universe, H₂ forms predominantly on the surface of dust grains (Gould & Salpeter 1963). On the other hand, CO forms in the gas phase via various reactions. Both species favour ‘shielded’ environments with a high column density of gas since they are dissociated by ultraviolet (UV) radiation. At high column densities, H₂ molecules can shield

UV radiation by their own absorption (Draine & Bertoldi 1996) (i.e. self-shielding). Since self-shielding of CO is weaker (Lee et al. 1996), CO forms in more embedded regions than H₂. Dust extinction also plays an important role in shielding dissociating radiation. Although CO emission is empirically known to trace H₂ in solar-metallicity environments, it is not obvious that this is generally true for galaxies (i) because these species have different formation mechanisms and the formation rates have different dependence on metallicity (Maloney & Black 1988), and (ii) because UV intensity and dust abundance vary in different stages of galaxy evolution.

For the purpose of deriving the H₂ abundance from an observed CO intensity, one assumes a CO-to-H₂ conversion factor, $X_{\text{CO}} \equiv N_{\text{H}_2}/W_{\text{CO}}$, where N_{H_2} is the H₂ column density, and W_{CO} is the intensity of the CO $J = 1 \rightarrow 0$ emission line integrated for the frequency (the frequency is often converted to the velocity shift in units of km s⁻¹). Another expression for the conversion factor, α_{CO} , is based on the column mass density (or surface mass density) of the molecular gas, $\Sigma_{\text{mol}} = 1.36 m_{\text{H}} (2N_{\text{H}_2})$, where 1.36 is a factor to account for the contribution of helium to the total mass. In this expression, the conversion factor is defined as $\alpha_{\text{CO}} \equiv \Sigma_{\text{mol}}/W_{\text{CO}}$. In this paper, we represent the CO-to-H₂ conversion factor by X_{CO} .

* E-mail: hirashita@asiaa.sinica.edu.tw

Deriving a reasonable CO-to-H₂ conversion factor is not easy. To observationally derive the CO-to-H₂ conversion factor, we need to know the H₂ content, which is not directly observed by its emission. The H₂ content (or the total column density or mass of a molecular cloud) is usually estimated indirectly through an estimate of the virial mass or a conversion from the dust far-infrared intensity to the total gas column density (see Bolatto et al. 2013, for a review). With such methods of obtaining the H₂ content, X_{CO} has been derived for various galaxies, mainly nearby ones. In particular, it has been found that X_{CO} depends on the metallicity (Wilson 1995; Arimoto et al. 1996; Israel 1997; Bolatto et al. 2008; Leroy et al. 2011; Hunt et al. 2015) as well as the density and temperature (Feldmann et al. 2012, hereafter FGK12; Narayanan et al. 2012).

As mentioned above, dust has an influence on both H₂ and CO abundances through shielding of UV dissociating photons and H₂ formation on dust surfaces. The metallicity dependence of X_{CO} mentioned above may reflect dust enrichment, which occurs simultaneously with metal enrichment (Lisenfeld & Ferrara 1998; Dwek 1998). Dust enrichment is one of the most important aspects for understanding the evolution of galaxies. Dust absorbs and scatters the stellar light and emit it in the far infrared, thereby shaping the spectral energy distribution (e.g. Yajima et al. 2014; Schaerer et al. 2015, for recent modelling). As mentioned above, grain surfaces provide a condition suitable for efficient formation of molecular hydrogen, which is an important coolant in low-metallicity clouds (e.g. Cazaux & Tielens 2004). Dust itself is also an important coolant in star formation, inducing the final fragmentation that determines the stellar mass (Omukai et al. 2005; Schneider et al. 2006).

Not only the dust abundance, but also the grain size distribution is important in various aspects. In particular, shielding of dissociating photons and H₂ formation on dust surfaces depend on the grain size distribution through the dependence of the surface area on the grain size. Asano et al. (2013) formulated the evolution of grain size distribution in a consistent manner with galaxy evolution. In their calculation, dust condensed in stellar ejecta [supernovae (SNe) and asymptotic giant branch star winds], dominate the grain size distribution at the early stage of galactic evolution (see also Valiante et al. 2009). These stellar sources form large ($\sim 0.1 \mu\text{m}$) grains, based on theoretical and observational evidence (see section 2.1 of Hirashita 2015, hereafter H15, for detailed references); thus, the dust is dominated by large grains at the early stage of galaxy evolution. As the system is enriched with dust, shattering as a result of grain-grain collision becomes efficient enough to increase the abundance of small grains. The increase of small grains drastically boosts the total grain surface area; as a consequence, grain growth by the accretion of gas-phase metals becomes the most important process for dust enrichment. Afterwards, the abundant small grains coagulate to form large grains. Nozawa et al. (2015) used the same model with a modification of incorporating the molecular cloud phase, which hosts strong accretion and coagulation, in addition to the originally included warm and cold phases. They explained not only the Milky Way extinction curve but also the extinction curve observed in a high-redshift quasar taken by Maiolino et al. (2004) (see also Gallerani et al. 2010).

Although the above recent models took into account

the full details of grain formation and processing mechanisms, there are still some uncertain free parameters regarding, especially, the time-scales of individual processes. The time-scales (or efficiencies) of accretion, shattering, and coagulation are strongly affected by the density structures in the ISM (Bekki 2015; McKinnon et al. 2016; Aoyama et al. 2016), since accretion and coagulation take place only in the dense and cold ISM while shattering occurs predominantly in the diffuse ISM (Yan et al. 2004; Asano et al. 2013). Therefore, to complement those detailed models, a parameter survey study is desirable; that is, we need to survey all the reasonable ranges of the time-scales, for the purpose of examining how sensitive the evolution of grain size distribution is to the assumed time-scales or for the purpose of finding the ranges of the time-scales that reproduce successfully the observed extinction curves (Bekki et al. 2015; Hou et al. 2016). However, a full treatment of grain size distribution requires a lot of computational time, and is not suitable for such a parameter survey study.

To make a parameter survey possible in a reasonable computational time, we adopt a simplified model developed by H15 to calculate the evolution of grain size distribution: H15 adopted a ‘two-size approximation’ approach, in which the grain sizes are represented by two sizes (large and small grains) separated around a radius of $0.03 \mu\text{m}$. This approximated model still includes all the above processes considered by Asano et al. (2013) but simply treats the production of or mass exchange between the small and large grain populations for the evolution of grain size distribution. H15 showed that this two-size approximation traces the same evolutionary behaviours of grain size distribution and extinction curve as presented in Asano et al. (2013, 2014). Therefore, H15 confirmed that the two-size approximation can be used as a simplified (or computationally cheap) version of the full treatment of grain size distribution. Bekki et al. (2015) applied the two-size approximation in combination with extinction curve calculations, finding that the variety of extinction curves among the Milky Way and the Large and Small Magellanic Clouds can be explained by different transportation efficiencies of small grains out of the galaxies. Indeed, they took advantage of the quickness of two-size approximation calculations to find optimum parameters that reproduce the observed extinction curves (see also Hou et al. 2016).

In this paper, utilizing the dust models mentioned above (specifically the two-size approximation in H15), we examine the effect of dust evolution on the abundances of H₂ and CO molecules. This enables us to examine the effect of dust evolution on the H₂ and CO abundances. In particular, we will focus on how the dust evolution, including the evolution of grain sizes, affects the metallicity dependence of X_{CO} . The dependence of H₂ formation rate on the evolution of grain size distribution has not been fully investigated: Yamasawa et al. (2011) incorporated the effect of grain size distribution on H₂ formation in a galaxy evolution model, but they only focused on the early stage of galaxy evolution. Since there have already been analytic models for H₂ formation (Hirashita & Ferrara 2005; Krumholz et al. 2008, 2009; McKee & Krumholz 2010), we focus on the effect of grain size, which has not been included in those models. The grain size distribution also affects the CO abundance through shielding of dissociating photons. Through this work, we not only understand or quantify the effect

of dust evolution on X_{CO} but also estimate how much the observational scatter in the X_{CO} –metallicity relation can be explained by the variation of dust evolution among galaxies. Since there are several processes driving the dust evolution, using a method suitable for a parameter survey such as the two-size approximation is crucial for the present work.

This paper is organized as follows. In Section 2, we model the dust evolution, the abundances of H_2 and CO, and the CO-to- H_2 conversion factor. In Section 3, we show the results for the basic predictions of our models. In Section 4, we further discuss the dependence on some physical components that cause major influences on the H_2 and CO abundances. In Section 5, we comment on some implications for various galaxy populations. Finally we give conclusions in Section 6. Throughout this paper, we adopt the typical conversion factor for the Milky Way as $X_{\text{CO}} = 2 \times 10^{20} \text{ cm}^{-2} \text{ K}^{-1} \text{ km}^{-1} \text{ s}$, which corresponds to $\alpha_{\text{CO}} = 4.3 M_{\odot} \text{ K}^{-1} \text{ km}^{-1} \text{ s pc}^2$ (Bolatto et al. 2013), and $Z_{\odot} = 0.02$ for the solar metallicity used for the metallicity normalization in the models (we adopt the same value as in H15).

2 MODEL

We first calculate how the dust content evolves as a function of metallicity to obtain the relation between dust-to-gas ratio and metallicity (\mathcal{D} – Z relation). In this calculation, we also trace the evolution of grain sizes by adopting the two-size approximation described below. Using the computed \mathcal{D} – Z relation, we calculate the molecular abundance of a single typical cloud in the galaxy. As a consequence, the model gives how the molecular abundances in a cloud is affected by the \mathcal{D} – Z relation.

2.1 Dust evolution

We use the two-size dust enrichment model developed by H15. In this model, to avoid heavy computation, the entire size range of dust grains is represented by small and large grains (roughly divided at $a \sim 0.03 \mu\text{m}$, where a is the grain radius), considering that various grain processing mechanisms work differently between these two grain populations. The model takes into account dust condensation in stellar ejecta, dust destruction in SN shocks, grain growth by accretion and coagulation, and grain disruption by shattering.

H15 considered the evolution of the abundances of small and large grains, and calculated the total mass of small/large grains divided by the total gas mass, referred to as the small/large-grain dust-to-gas ratio. We denote the small- and large-grain dust-to-gas ratios as \mathcal{D}_s and \mathcal{D}_l , respectively. The total dust-to-gas ratio is the sum of these two components as $\mathcal{D} = \mathcal{D}_s + \mathcal{D}_l$. After applying the instantaneous recycling approximation (Tinsley 1980), the evolutions of \mathcal{D}_s and \mathcal{D}_l are described in terms of metallicity evolution as (see H15 for the derivation)

$$\mathcal{D}_l \frac{d\mathcal{D}_l}{dZ} = f_{\text{in}}(\mathcal{R}Z + \mathcal{Y}_Z) + \beta_{\text{co}}\mathcal{D}_s - (\beta_{\text{SN}} + \beta_{\text{sh}} + \mathcal{R})\mathcal{D}_l, \quad (1)$$

$$\mathcal{D}_s \frac{d\mathcal{D}_s}{dZ} = \beta_{\text{sh}}\mathcal{D}_l - (\beta_{\text{SN}} + \beta_{\text{co}} + \mathcal{R} - \beta_{\text{acc}})\mathcal{D}_s, \quad (2)$$

where Z is the metallicity, f_{in} is the dust condensation efficiency of metals in the stellar ejecta, \mathcal{R} is the returned fraction of gas from stars, \mathcal{Y}_Z is the mass fraction of newly produced metals by stars, and β_{SN} , β_{sh} , β_{co} and β_{acc} indicate the efficiencies (explained below) of SN shock destruction, shattering, coagulation and accretion, respectively. Note that these efficiencies (referred to as β s) depend on \mathcal{D}_s or \mathcal{D}_l except β_{SN} (H15). The right-hand side of equation (1) represents the stellar dust production [$f_{\text{in}}(\mathcal{R}Z + \mathcal{Y}_Z)$; note that dust grains supplied by stars are assumed to be large; see H15 and references therein], the increase by coagulation of small grains ($\beta_{\text{co}}\mathcal{D}_s$), the decreases by SN destruction and shattering ($\beta_{\text{SN}}\mathcal{D}_l$ and $\beta_{\text{sh}}\mathcal{D}_l$, respectively), and the dilution of dust-to-gas ratio by returned gas from stars ($\mathcal{R}\mathcal{D}_l$). Equation (2) shows the increase of small grains: the shattering and coagulation terms in equation (2) have the opposite sign to those in equation (1), since shattering is source and coagulation is sink for small grains. The increase of dust abundance by accretion ($\beta_{\text{acc}}\mathcal{D}_s$) only appears in equation (2) based on the argument that accretion is much more efficient for small grains than for large grains because small grains have much larger surface-to-volume ratio (Hirashita & Kuo 2011; Asano et al. 2013).

The efficiencies denoted as β s are defined as $\beta_{\text{SN}} \equiv \tau_{\text{SF}}/\tau_{\text{SN}}$, $\beta_{\text{sh}} \equiv \tau_{\text{SF}}/\tau_{\text{sh}}$ and $\beta_{\text{co}} \equiv \tau_{\text{SF}}/\tau_{\text{co}}$, where $\tau_{\text{SF}} \equiv M_{\text{gas}}/\psi$ (M_{gas} is the total gas mass in the galaxy and ψ is the star formation rate) is the star formation time-scale, and the shattering and coagulation time-scales are proportional to the dust-to-gas ratios, since shattering and coagulation are collisional processes:

$$\tau_{\text{sh}} = \tau_{\text{sh},0} \left(\frac{\mathcal{D}_l}{\mathcal{D}_{\text{MW},l}} \right)^{-1}, \quad (3)$$

$$\tau_{\text{co}} = \tau_{\text{co},0} \left(\frac{\mathcal{D}_s}{\mathcal{D}_{\text{MW},s}} \right)^{-1}, \quad (4)$$

where the time-scales are normalized to $\tau_{\text{sh},0}$ and $\tau_{\text{co},0}$, which are the values at the MW dust-to-gas ratio, $\mathcal{D}_{\text{MW},l} = 0.007$ and $\mathcal{D}_{\text{MW},s} = 0.003$ (H15). The accretion efficiency β_{acc} is regulated by the lifetime of dense clouds (τ_{cl}) and the metallicity. Accretion is more efficient for longer τ_{cl} . For β_{acc} , we need the averaged values of a^{ℓ} ($\ell = 1, 2, \text{ and } 3$) (see Appendix A) because accretion is a surface process in which the grain size, surface and volume play an important role. The calculation of β_{acc} is explained in Appendix B.

By solving equations (1) and (2), we obtain the relation between dust-to-gas ratio and metallicity (\mathcal{D} – Z relation). Below, we consider a cloud whose column density is typical of Galactic molecular clouds, and calculate the H_2 and CO abundances in the cloud based on the dust abundance given as a function of metallicity by the above \mathcal{D} – Z relation.

2.2 H_2 abundance

We consider a cloud with a hydrogen column density of $N_{\text{H}} \sim 10^{22} \text{ cm}^{-2}$ (typical of Galactic molecular clouds) under a given metallicity. We assume that this cloud has small- and large-grain dust-to-gas ratios $\mathcal{D}_s(Z)$ and $\mathcal{D}_l(Z)$ calculated by the model in Section 2.1. The H_2 abundance is assumed to be determined by the balance between formation and dissociation (this equilibrium assumption is discussed at the end of this subsection). The H_2 formation rate is propor-

tional to the local density represented by the number density of hydrogen nuclei n_{H} . For dissociation, the column density of hydrogen nuclei N_{H} as well as the UV radiation field χ is important for shielding of dissociating photons [χ is the UV radiation field intensity at the Lyman-Werner (LW) band normalized to the solar neighbourhood value derived by [Habing 1968](#), 3.2×10^{-20} erg s $^{-1}$ cm $^{-2}$ Hz $^{-1}$ sr $^{-1}$; see also [Hirashita & Ferrara 2005](#)]. Expressing the UV radiation field with a single parameter χ means that we neglect the dependence of stellar UV spectrum (or hardness) on metallicity. As shown later, the variation of UV radiation has a large influence on the molecular abundances at low metallicity, where we are not much interested in the CO abundance since it is too low to be detected. The H $_2$ abundance at low metallicity could be affected by the variation of UV spectrum. However, according to [Schaerer \(2002\)](#), with a fixed star formation rate, the H $_2$ dissociation rate only differs by a factor of 1.5 between low ($\sim 1/50 Z_{\odot}$) and solar metallicities, while we will vary χ by orders of magnitude in this paper. Thus, we simply concentrate on the variation of χ (UV intensity) and neglect the variation of hardness.

Under a given set of ($n_{\text{H}}, N_{\text{H}}, \chi$), we calculate the H $_2$ fraction, f_{H_2} achieved as a result of the equilibrium between the formation on dust and the dissociation by UV (LW band) radiation. The H $_2$ fraction is defined in such a way that $f_{\text{H}_2} N_{\text{H}}/2$ gives the column density of H $_2$. The rates of formation and dissociation are given in what follows.

The increasing rate of f_{H_2} by H $_2$ formation on dust is described as

$$\left[\frac{df_{\text{H}_2}}{dt} \right]_{\text{form}} = 2 \sum_i (1 - f_{\text{H}_2}) R_{\text{H}_2, \text{dust}}^i n_{\text{H}}, \quad (5)$$

where the rate coefficient $R_{\text{H}_2, \text{dust}}^i$ (superscript i indicates small or large grains; i.e. $i = \text{s}$ or $i = \text{l}$) is introduced. The rate coefficient, which depends on the dust-to-gas ratio, is determined by ([Yamasawa et al. 2011](#))

$$R_{\text{H}_2, \text{dust}}^i = \frac{3 \mathcal{D}_i \mu m_{\text{H}} S_{\text{H}} \bar{v} \langle a^2 \rangle_i}{8s \langle a^3 \rangle_i}, \quad (6)$$

where s is the material density of dust, m_{H} is the atomic mass of hydrogen, \bar{v} is the mean thermal speed, S_{H} is the probability of a hydrogen atom reacting with another hydrogen atom on the dust surface to form H $_2$, and $\langle a^2 \rangle_i$ and $\langle a^3 \rangle_i$ are the second and third moments with subscript i indicating small or large grains (Appendix A). We adopt $s = 3.3$ g cm $^{-3}$ ([Draine & Lee 1984](#)) and $\mu = 1.4$. Adopting instead $s \sim 2$ g cm $^{-3}$ appropriate for carbonaceous dust does not affect our conclusions below. We also fix $S_{\text{H}} = 0.3$: such a high value is reasonable to adopt since we are particularly interested in H $_2$ formation in cold and shielded environments ([Hollenbach & McKee 1979](#)). The thermal speed is estimated as ([Spitzer 1978](#))

$$\bar{v} = \sqrt{\frac{8k_{\text{B}} T_{\text{gas}}}{\pi m_{\text{H}}}}, \quad (7)$$

where k_{B} is the Boltzmann constant, and T_{gas} is the kinetic temperature of the gas.

The changing rate of f_{H_2} by photodissociation is estimated as

$$\left[\frac{df_{\text{H}_2}}{dt} \right]_{\text{diss}} = -R_{\text{diss}} f_{\text{H}_2}, \quad (8)$$

where the rate coefficient R_{diss} is given by ([Hirashita & Ferrara 2005](#))

$$R_{\text{diss}} = 4.4 \times 10^{-11} \chi S_{\text{shield, H}_2} S_{\text{shield, dust}}, \quad (9)$$

with $S_{\text{shield, H}_2}$ and $S_{\text{shield, dust}}$ being the correction factors for H $_2$ self-shielding and dust extinction, respectively. We adopt the following form for S_{shield} ([Draine & Bertoldi 1996](#); [Hirashita & Ferrara 2005](#)):

$$S_{\text{shield, H}_2} = \min \left[1, \left(\frac{\frac{1}{2} f_{\text{H}_2} N_{\text{H}}}{10^{14} \text{ cm}^{-2}} \right)^{-0.75} \right], \quad (10)$$

and

$$S_{\text{shield, dust}} = \exp \left(- \sum_i \tau_{\text{LW}, i} \right), \quad (11)$$

where $\tau_{\text{LW}, i}$ is the optical depth of dust component i at the LW band. This optical depth is estimated as

$$\tau_{\text{LW}, i} = \left(\frac{\tau_{\text{LW}}}{N_{\text{H}}} \right)_{0.01, i} \left(\frac{\mathcal{D}_i}{0.01} \right) N_{\text{H}}, \quad (12)$$

where $(\tau_{\text{LW}}/N_{\text{H}})_{0.01, i}$ is the optical depth of dust component i (again, $i = \text{s}$ or $i = \text{l}$ for small and large grains, respectively) for $\mathcal{D}_i = 0.01$ at the LW band, normalized to the hydrogen column density. [H15](#) showed that, with $\mathcal{D}_{\text{s}} = 0.003$ and $\mathcal{D}_{\text{l}} = 0.007$, which are appropriate for the Milky Way, the Milky Way extinction curve is reproduced with a mass ratio of silicate-to-carbonaceous dust of 0.54 : 0.46. We fix this silicate-to-carbonaceous dust ratio in calculating the extinction for simplicity. If we adopt the representative wavelength for the LW band as 1000 Å, we obtain $(\tau_{\text{LW}}/N_{\text{H}})_{0.01, \text{s}} = 8.2 \times 10^{-21}$ cm 2 and $(\tau_{\text{LW}}/N_{\text{H}})_{0.01, \text{l}} = 2.3 \times 10^{-21}$ cm 2 . Fixing the silicate-to-carbonaceous dust abundance ratio does not affect our results significantly. Grain composition is indeed suggested to be different in different galaxies: studies on extinction curves indicate that the dust composition in the Small Magellanic Cloud (SMC) is dominated by silicate with little contribution from carbonaceous dust ([Pei 1992](#); [Weingartner & Draine 2001](#)). Under the same grain size distribution, the extinction curve composed purely of silicate has an enhancement by a factor of ~ 1.4 around 1000 Å compared with the silicate-graphite mixture that reproduces the Milky Way extinction curve ([Pei 1992](#)). As we see later, dust extinction is important for CO formation, but considering the sensitive dependence of CO abundance on dust-to-gas ratio, difference in τ_{LW} only by a factor of 1.4 does not affect our discussions and conclusions in this paper. Although the above extinction curve studies cannot exclude a possibility of other dust species than silicate and carbonaceous dust (note that [Tchernyshyov et al. 2015](#) suggest that dust containing no silicon atom should exist in some regions in the SMC based on their study of elemental depletion), we concentrate on the change of dust abundance \mathcal{D}_i by fixing the coefficient $(\tau_{\text{LW}}/N_{\text{H}})_{0.01, i}$ in this paper.

In the above, we assumed the equilibrium between H $_2$ formation and destruction. Thus, we implicitly assume that the cloud has a longer lifetime than the H $_2$ formation time-scale. The H $_2$ formation time-scale, τ_{H_2} , is estimated as

$$\tau_{\text{H}_2} = \frac{f_{\text{H}_2}}{[df_{\text{H}_2}/dt]_{\text{form}}}. \quad (13)$$

If we approximate the reaction rate in equation (6) by

using an intermediate value of $\langle a^3 \rangle_i / \langle a^2 \rangle_i \sim 0.01 \mu\text{m}$ between large and small grains (Table A1) and by replacing \mathcal{D}_i with \mathcal{D} , we obtain (omitting superscript i) $R_{\text{H}_2, \text{dust}} \sim 3.7 \times 10^{-17} (\mathcal{D}/0.01) (T/10 \text{ K})^{1/2} (n_{\text{H}}/10^3 \text{ cm}^{-3}) \text{ cm}^3 \text{ s}^{-1}$, which leads to $\tau_{\text{H}_2} \sim f_{\text{H}_2} / (R_{\text{H}_2, \text{dust}} n_{\text{H}}) \sim 8.7 \times 10^5 f_{\text{H}_2} (\mathcal{D}/0.01)^{-1} (T/10 \text{ K})^{-1/2} (n_{\text{H}}/10^3 \text{ cm}^{-3})^{-1} \text{ yr}$. This time-scale can be compared with the free-fall time estimated as $\tau_{\text{ff}} \sim 1.4 \times 10^6 (n_{\text{H}}/10^3 \text{ cm}^{-3})^{-1/2} \text{ yr}$. We find that $\tau_{\text{H}_2} < \tau_{\text{ff}}$ is satisfied if the dust-to-gas ratio is near to the Milky Way value. Thus, if we consider a typical molecular cloud, the equilibrium assumption on the H_2 abundance is reasonable, since the time-scale of gravitational evolution occurs on a longer time-scale than the reaction time-scale (although the reaction may be non-equilibrium for small-scale structures; Gibson et al. 2015). However, if the dust-to-gas ratio is significantly lower than the Milky Way value, the equilibrium assumption should be considered carefully, since τ_{H_2} becomes long in proportion to \mathcal{D}^{-1} (see also Hu et al. 2016). The assumption of equilibrium is yet justified if the molecular cloud is sustained against the free fall or if the resulting f_{H_2} is significantly smaller than unity. For example, if the molecular cloud is sustained for a few free-fall times as indicated for nearby molecular clouds (e.g. Ward-Thompson et al. 2007, although this is still debated), the equilibrium assumption for H_2 formation is reasonable down to $\mathcal{D} \sim 0.001$. In terms of the comparison with observations, we are mainly interested in objects with $\mathcal{D} \gtrsim 0.001$, for which CO could be detected. Nevertheless, we should keep in mind that our results around $\mathcal{D} \sim 0.001$, roughly corresponding to $Z \sim 0.1 Z_{\odot}$ are interpreted carefully, and that calculations taking into account non-equilibrium H_2 formation is desirable for a future study.

2.3 CO abundance

The CO abundance is determined by a complicated chemical network that includes a lot of reactions. For example, Glover et al. (2010) treated a chemical network composed of ~ 200 reactions. Since calculations of such a large chemical network are generally time-consuming, performing full chemical calculations for the CO abundance with a large number of cases for dust evolution at various metallicities is not realistic. Therefore, we utilize CO abundance data already calculated for various physical conditions by Glover & Mac Low (2011, hereafter GM11) (see also Shetty et al. 2011). They calculated spatially resolved H_2 and CO abundances over a region of 5–20 pc using dynamical simulations of magnetized turbulence coupled with a chemical network for H_2 and CO and a treatment of photodissociation. We follow the method used by FGK12, who adopted the calculation results in GM11. Below we explain the calculation method of CO abundance.

Before we explain our formulation, we need to relate the column density with the local density, since the reaction rate is determined by the local density. In the original formulation in FGK12, the dependences on n_{H} and N_{H} are both absorbed in A_V by imposing $A_V \propto n_{\text{H}} \propto N_{\text{H}}$. In this paper, the proportionality constant between A_V and N_{H} is given consistently with our model, while we use the relation given in FGK12 for A'_V and N'_{H} (see below), where we put a prime to the quantities calculated in GM11 to distinguish them from the quantities calculated in our model. We al-

ways adopt $N_{\text{H}}/n_{\text{H}} = N'_{\text{H}}/n'_{\text{H}}$ to make the following equations solvable (following FGK12).

The CO abundance x_{CO} is defined as the number ratio of CO molecules to hydrogen nuclei. We assume, following FGK12, that the CO abundance is determined by the dust extinction and the radiation field under a given metallicity; thus, we write the CO abundance as $x_{\text{CO}} = x_{\text{CO}}(A_V, \chi, Z)$.

Now let us formulate the estimation method of the CO abundance. We utilize the calculation results in GM11 to estimate x_{CO} . GM11 provide CO fraction x'_{CO} at $\chi' = 1.7$.¹

Following FGK12, we start with the equilibrium between dissociation and formation of CO in the two systems that realize CO abundances of x_{CO} and x'_{CO} (recall that the quantities with a prime mean those obtained in GM11's simulation):

$$x_{\text{CO}} \chi S_{\text{dust}}(A_{V, \text{eff}}) S_{\text{H}_2}(N_{\text{H}_2}) S_{\text{CO}}(N_{\text{CO}}) = n_{\text{H}} \sum_{i,j} \mathcal{R}_{i,j} x_i x_j, \quad (14)$$

and

$$1.7 x'_{\text{CO}} S_{\text{dust}}(A'_V) S_{\text{H}_2}(N'_{\text{H}_2}) S_{\text{CO}}(N'_{\text{CO}}) = n'_{\text{H}} \sum_{i,j} \mathcal{R}_{i,j} x'_i x'_j, \quad (15)$$

where $\mathcal{R}_{i,j}$ is the reaction rates of CO formation from species i and j , the abundances of which are denoted as x_i and x_j (or x'_i and x'_j), respectively. As mentioned in FGK12, it is plausible that $x_i \sim x'_i$ and $x_j \sim x'_j$ under $x_{\text{CO}} = x'_{\text{CO}}$. Thus, we expect that the left-hand side of equation (14) divided by n_{H} is equal to the left-hand side of equation (15) divided by n'_{H} . Recalling that we adopt $n_{\text{H}}/n'_{\text{H}} = N_{\text{H}}/N'_{\text{H}}$ and using $x_{\text{CO}} = x'_{\text{CO}}$, we obtain

$$\chi S_{\text{dust}}(A_{V, \text{eff}}) S_{\text{H}_2}(N_{\text{H}_2}) S_{\text{CO}}(N_{\text{CO}}) / N_{\text{H}} = 1.7 S_{\text{dust}}(A'_V) S_{\text{H}_2}(N'_{\text{H}_2}) S_{\text{CO}}(N'_{\text{CO}}) / N'_{\text{H}}, \quad (16)$$

where $S_{\text{dust}}(A_V)$, $S_{\text{H}_2}(N_{\text{H}_2})$, and $S_{\text{CO}}(N_{\text{CO}})$ are the shielding factors of CO-dissociating photons ($1 - S$ is the fraction of shielded CO-dissociating radiation by each species) by dust, H_2 , and CO, respectively, and $A_{V, \text{eff}} = A_{1000} / 4.7$ is the effective V -band extinction. The shielding functions S 's are taken from Lee et al. (1996). To obtain $A_{V, \text{eff}}$, we first obtain $A_{1000} \simeq 1.086 \sum_i \tau_{\text{LW}, i}$ using equation (12). We convert this to $A_{V, \text{eff}}$ with the above relation, where the factor 4.7 comes from the Milky Way extinction curve (Pei 1992).

Equation (16) is the one we solve to obtain the CO abundance. Note that all the quantities on the left-hand side in equation (16) are given by our simulation except for $N_{\text{CO}} = x_{\text{CO}} N_{\text{H}} = x'_{\text{CO}} N_{\text{H}}$ while those on the right-hand side are given as a function of A'_V as we see below. Because x'_{CO} is a function of A'_V as we see below (thus, with the assumption of $x_{\text{CO}} = x'_{\text{CO}}$, x_{CO} is also a function of A'_V), equation (16) is an equation for A'_V . Once we obtain A'_V , we calculate $x_{\text{CO}} = x'_{\text{CO}}(A'_V)$.

Now we explain how N'_{H_2} and N'_{CO} are expressed as a function of A'_V . Based on GM11's result, we adopt the following fitting formulae:

$$f'_{\text{H}_2} = 1 - \exp(-0.45 A'_V), \quad (17)$$

¹ The Milky Way interstellar radiation field adopted by GM11 is based on Draine (1978)'s estimate, which corresponds to $\chi = 1.7$. As shown later, we can practically regard x'_{CO} as a function of A'_V .

and

$$\log x'_{\text{CO}} = -7.64 + 3.89 \log A'_V, \quad (18)$$

where the H_2 fraction f'_{H_2} is related to N'_{H_2} as $N'_{\text{H}_2} = f'_{\text{H}_2} N'_{\text{H}}/2$, and

$$N'_{\text{H}} = \frac{A'_V}{5.348 \times 10^{-22} (Z'/Z_{\odot}) \text{ cm}^2} \quad (19)$$

in GM11's formulation (we adopt $Z' = Z$). Note that these relations (equation 17–19) do not hold among f_{H_2} , x_{CO} , N_{H} and A_V because physical conditions such as dust properties and radiation field are different between our models and GM11's calculations. We also use $N_{\text{H}_2} = f_{\text{H}_2} N_{\text{H}}/2$ and $N_{\text{CO}} = x_{\text{CO}} N_{\text{H}}$, and use f_{H_2} calculated in Section 2.2. As mentioned above, we are looking for a solution that satisfies $x_{\text{CO}} = x'_{\text{CO}}$. Thus, equation (16) is rewritten as

$$\chi S_{\text{dust}}(A_{V,\text{eff}}) S_{\text{H}_2}(f_{\text{H}_2} N_{\text{H}}/2) S_{\text{CO}}(x'_{\text{CO}} N_{\text{H}})/N_{\text{H}} \\ = 1.7 S_{\text{dust}}(A'_V) S_{\text{H}_2}(f'_{\text{H}_2} N'_{\text{H}}/2) S_{\text{CO}}(x'_{\text{CO}} N'_{\text{H}})/N'_{\text{H}}, \quad (20)$$

where f'_{H_2} , x'_{CO} , and N'_{H} are all functions of A'_V through equations (17), (18), and (19), respectively. Note that N_{H} is a given parameter, and that $A_{V,\text{eff}}$ and f_{H_2} are calculated by the model. Thus, we solve equation (20) to obtain A'_V , which is translated into the CO abundance $x'_{\text{CO}} = x_{\text{CO}}$ through equation (18).

We impose an upper limit $x_{\text{C}} = 1.41 \times 10^{-4} Z/Z_{\odot}$ (carbon abundance) for x_{CO} ; that is, if the obtained x_{CO} is larger than the carbon abundance, we adopt $x_{\text{CO}} = x_{\text{C}}$. This only occurs at super-solar metallicities in our models.

2.4 CO-to- H_2 conversion factor

Using the quantities calculated above, we finally calculate the CO-to- H_2 conversion factor:

$$X_{\text{CO}} = N_{\text{H}_2}/W_{\text{CO}}. \quad (21)$$

We compute W_{CO} using the following expression (GM11):

$$W_{\text{CO}} = T_{\text{r}} \Delta v \int_0^{\tau_{10}} 2\beta(\tau) d\tau, \quad (22)$$

where T_{r} is the observed radiation temperature (calculated later in equation 25), Δv is the velocity width of the CO line, τ_{10} is the optical depth of the CO $J = 1 \rightarrow 0$ transition, and $\beta(\tau)$ is the photon escape probability as a function of the optical depth. The escape probability is estimated as (Tielens 2005)

$$\beta(\tau) = \begin{cases} [1 - \exp(-2.34\tau)]/(4.68\tau) & \text{if } \tau \leq 7; \\ 1/(4\tau[\ln(\tau/\sqrt{\pi})]^{1/2}) & \text{if } \tau > 7. \end{cases} \quad (23)$$

The optical depth τ_{10} is estimated as (Tielens 2005; FGK12)

$$\tau_{10} = 1.4 \times 10^{-16} (1 - e^{-5.5/T_{\text{gas}}}) \left(\frac{\Delta v}{3 \text{ km s}^{-1}} \right)^{-1} \left(\frac{N_{\text{CO}}}{\text{cm}^{-2}} \right). \quad (24)$$

The radiation temperature of the CO $J = 1 \rightarrow 0$ transition with the subtraction of the cosmic microwave background (CMB) taken into account is calculated by

$$T_{\text{r}} = 5.5 \left(\frac{1}{e^{5.5/T_{\text{gas}}} - 1} - \frac{1}{e^{5.5/T_{\text{CMB}}} - 1} \right) \text{ K}, \quad (25)$$

Table 1. Parameter ranges surveyed for dust evolution.

Parameter	Process	Minimum	Maximum	Fiducial
f_{in}	stellar ejecta	0.01	0.1	0.1
β_{SN}	SN destruction	4.8	19	9.65
τ_{cl}	accretion	10^6 yr	10^8 yr	10^7 yr
$\tau_{\text{sh},0}$	shattering	10^7 yr	10^9 yr	10^8 yr
$\tau_{\text{co},0}$	coagulation	10^6 yr	10^8 yr	10^7 yr
τ_{SF}	star formation	0.5 Gyr	50 Gyr	5 Gyr

where $T_{\text{CMB}} = 2.73(1+z)$ is the CMB temperature (z is the redshift of the galaxy considered; we adopt $z = 0$ in this paper). For the velocity width, we simply adopt the typical value adopted in FGK12, $\Delta v = 3 \text{ km s}^{-1}$, partly because our models are based on their model, partly because a direct comparison with their model is possible (i.e. our models are ‘calibrated’ by their model). Using equation (22) and the H_2 column density calculated in Section 2.2, we finally obtain the CO-to- H_2 conversion factor, X_{CO} , by equation (21).

2.5 Choice of parameter values

For the dust evolution model, we adopt $\mathcal{R} = 0.25$ and $\mathcal{Z} = 0.013$ (Hirashita & Kuo 2011). For the parameters governing the dust evolution, we adopt the same ranges as adopted in H15 as listed in Table 1.

As assumed in Section 2.3, we give χ and N_{H} for the physical condition of the cloud at a given Z . Although n_{H} is not essential to our formulation for the CO abundance, it is necessary in calculating the H_2 abundance. Whenever necessary, we adopt $n_{\text{H}} = 10^3 \text{ cm}^{-2}$, which is appropriate for the molecular clouds in the Milky Way (but not necessarily ‘molecular’ in galaxies with higher χ or lower Z than in the Milky Way) (Hirashita & Kuo 2011). For the column density, we investigate a range of $N_{\text{H}} = 10^{21}\text{--}10^{23} \text{ cm}^{-2}$, corresponding to surface densities of $10\text{--}10^3 \text{ M}_{\odot} \text{ pc}^{-2}$. This covers the range of surface densities of giant molecular clouds in various environments (e.g. Bolatto et al. 2013). For the UV intensity normalized to the Habing (1968) value, Hirashita & Ferrara (2005) derived the relation between χ and the surface density of SFR (Σ_{SFR}) by assuming that the UV luminosity traces the current star formation rate as

$$\Sigma_{\text{SFR}} = 1.7 \times 10^{-3} \chi \text{ M}_{\odot} \text{ yr}^{-1} \text{ kpc}^{-2}. \quad (26)$$

We survey a range of $\chi = 1.7\text{--}170$ (1–100 times the Galactic value), corresponding to $\Sigma_{\text{SFR}} = 2.9 \times 10^{-3}\text{--}0.29 \text{ M}_{\odot} \text{ yr}^{-1} \text{ kpc}^{-2}$, which roughly covers the range of nearby disc galaxies (Kennicutt 1998) (see also Section 5.2). Starburst galaxies have Σ_{SFR} 10–100 times higher Σ_{SFR} (Kennicutt 1998), thus χ . We consider such extreme values of χ later in Section 5.3. In Table 2, we list the ranges and fiducial values of N_{H} and χ .

3 RESULTS

3.1 Basic properties

Here we investigate the general evolution of H_2 and CO abundances under various conditions. We adopt the fiducial values for the parameters of dust evolution and cloud

Table 2. Parameter ranges for the physical condition of clouds.

Parameter	Minimum	Maximum	Fiducial
N_{H}	10^{21} cm^{-2}	10^{23} cm^{-2}	10^{22} cm^{-2}
χ	1.7	170	1.7

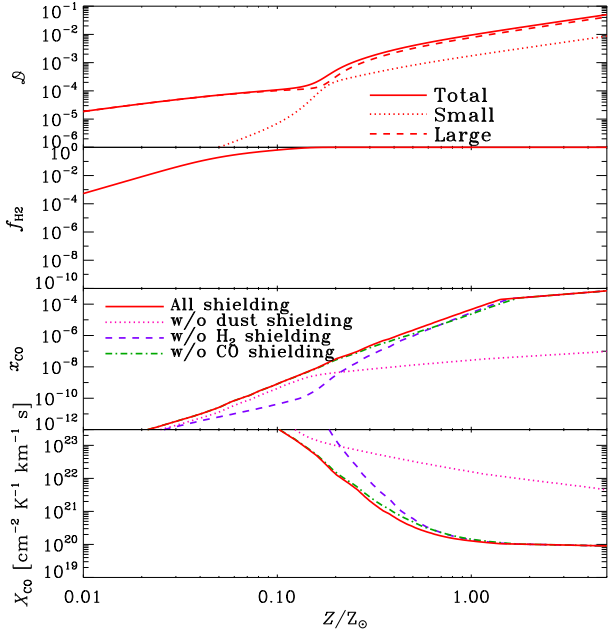


Figure 1. Quantities of interest as a function of metallicity. Panels from upper to lower show the dust-to-gas ratio (\mathcal{D}), H_2 fraction (f_{H_2}), CO fraction (x_{CO}) and CO-to- H_2 conversion factor (X_{CO}). For the dust-to-gas ratio, the small and large grain components are shown by the dotted and dashed lines, respectively, and the total dust-to-gas ratio is shown by the solid line. For x_{CO} and X_{CO} , the cases without either dust shielding (dotted), H_2 shielding (dashed), or CO self-shielding (dot-dashed) are also shown. X_{CO} is shown only when $x_{\text{CO}} > 10^{-10}$.

properties (Tables 1 and 2). In Fig. 1, we show the metallicity dependence of the quantities investigated in this paper, namely, the dust-to-gas ratio (\mathcal{D}), H_2 fraction (f_{H_2}), CO fraction (x_{CO}) and CO-to- H_2 conversion factor (X_{CO}). X_{CO} is only shown where $x_{\text{CO}} > 10^{-10}$, below which detection of CO is impossible in any case.

H_{15} already investigated and discussed the \mathcal{D} - Z relation, which is briefly described in what follows. Dust is supplied by stars at low metallicities, and is dominated by large grains. Small grains gradually increase because of shattering of large grains. At a certain point, the increase of small grains is accelerated because of accretion, which induces the increase of large grains as well through coagulation. As a consequence, the total dust abundance steeply increases as seen around $Z \sim 0.1$ – $0.2 Z_{\odot}$. After that, the dust-to-gas ratio gradually increases because of the metal enrichment; at this stage, the dust-to-gas ratio is determined by the balance between accretion and SN destruction.

The H_2 fraction, f_{H_2} , also increases as the dust-to-gas

ratio increases. A fully molecular condition is realized at $Z \gtrsim 0.1 Z_{\odot}$. Thus, a cloud with a typical density and column density of Milky Way ‘molecular’ clouds is not fully molecular below metallicity $0.1 Z_{\odot}$. The CO fraction, x_{CO} , also increases associated with the increase of dust-to-gas ratio. To understand what drives the increase of x_{CO} , we also show the cases without either dust shielding, H_2 shielding, or CO self-shielding in the third window in Fig. 1. The prediction without H_2 shielding underproduces the CO abundance at low metallicity $\lesssim 0.2 Z_{\odot}$, which indicates that H_2 shielding is important for CO formation. This is associated with the metallicity at which the cloud becomes fully molecular. At $Z \gtrsim 0.2 Z_{\odot}$, the main shielding component changes to dust: If we do not include dust shielding, the CO abundance remains as low as $\sim 10^{-6}$ – 10^{-5} . Dust shielding becomes important after the dust abundance is increased by accretion. Self-shielding of CO has an influence on the CO abundance only around solar metallicity, but its contribution is minor. The CO abundance, x_{CO} cannot be larger than the carbon abundance (x_{C}); thus, at $Z \gtrsim 2 Z_{\odot}$, x_{CO} is limited by the carbon abundance.

The CO-to- H_2 conversion factor, X_{CO} is sensitive to metallicity. This is particularly because there is a metallicity range where the cloud is rich in H_2 but is not rich in CO at $Z \gtrsim 0.1 Z_{\odot}$. Around solar metallicity, X_{CO} is near to the value observed in the Milky Way ($\sim 2 \times 10^{20} \text{ cm}^{-2} \text{K}^{-1} \text{km}^{-1} \text{s}$; Bolatto et al. 2013). Above solar metallicity, X_{CO} is not sensitive to metallicity because the CO $J = 1 \rightarrow 0$ line is optically thick. We also show the metallicity dependence of the CO-to- H_2 conversion factor without one of the shielding mechanisms. H_2 shielding has an influence on the slope of the X_{CO} - Z relation, since it has a larger impact on the CO abundance at low metallicity as discussed above. Dust shielding has a dramatic impact: X_{CO} is two orders of magnitude higher than the Milky way value at solar metallicity if we do not include dust shielding. CO self-shielding has little influence on X_{CO} .

3.2 Dependence on the cloud parameters

We investigate the dependence on the cloud parameters listed in Table 2 (i.e. N_{H} and χ). In Fig. 2, we show the variation of the quantities of interest as a function of metallicity. Note that the \mathcal{D} - Z relation is not affected by the change of those parameters.

In Fig. 2a, we show the dependence on the column density (N_{H}). Because of stronger self-shielding, f_{H_2} is larger for a larger N_{H} ($f_{\text{H}_2} \propto N_{\text{H}}^3$ for the self-shielded regime as long as $f_{\text{H}_2} \ll 1$; Hirashita & Ferrara 2005). The increase of dust abundance around $Z \sim 0.1 Z_{\odot}$ is important to raise the H_2 fraction for $N_{\text{H}} = 10^{21} \text{ cm}^{-2}$; thus, the increase of dust abundance by accretion is important to make the cloud molecule-rich at low column densities. The CO abundance is very sensitive to N_{H} ; at $Z \lesssim 0.1 Z_{\odot}$, the CO abundance is governed by H_2 shielding, while at higher metallicities, it is regulated by dust shielding (Section 3.1). In the case of $N_{\text{H}} = 10^{23} \text{ cm}^{-2}$, the rapid change of x_{CO} around $Z \sim 0.1 Z_{\odot}$ is due to the rapid increase of dust abundance (or dust shielding). The CO-to- H_2 conversion factor, X_{CO} , drops to $10^{21} \text{ cm}^{-2} \text{K}^{-1} \text{km}^{-1} \text{s}$ even at $Z \sim 0.2 Z_{\odot}$ in the case of $N_{\text{H}} = 10^{23} \text{ cm}^{-2}$, while it does not drop further because of high CO optical depth.

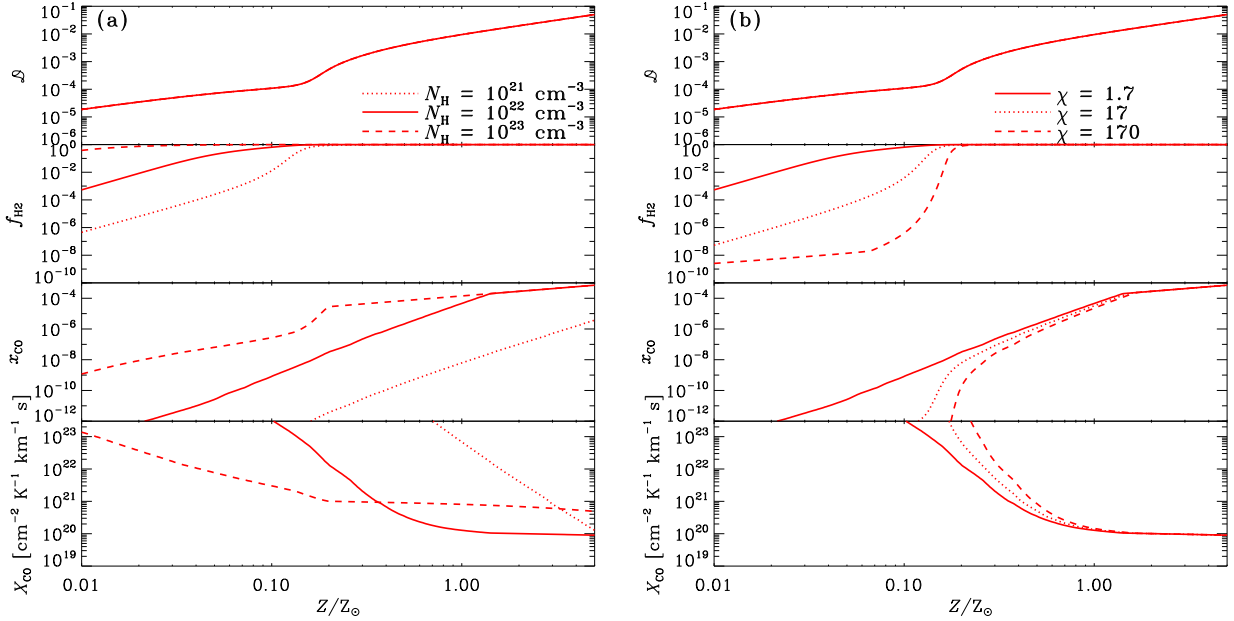


Figure 2. Same as Fig. 1 but with the following parameters changed: (a) $N_{\text{H}} = 10^{21}$, 10^{22} , and 10^{23} cm^{-2} for the dotted, solid, and dashed lines, respectively, with $\chi = 1.7$. (The solid line always shows the fiducial case in all the figures in this paper.) (b) $\chi = 1.7$, 17, and 170 for the solid, dotted, and dashed lines, respectively, with $N_{\text{H}} = 10^{22}$ cm^{-2} . We fix the values of the parameters other than the changed parameter at the fiducial values listed in Table 2. We adopt the dust evolution model characterized by the fiducial parameters in Table 1.

In contrast, X_{CO} for $N_{\text{H}} = 10^{21}$ cm^{-2} is much higher than the Galactic value ($\sim 2 \times 10^{20}$ cm^{-2} K^{-1} km^{-1} s) because of low dust shielding. Around solar metallicity, the case with $N_{\text{H}} = 10^{22}$ cm^{-2} has the smallest X_{CO} among the three column densities. This is consistent with the theoretical expectation by FGK12 (see their figure 3): as mentioned above, at $N_{\text{H}} \lesssim 10^{22}$ cm^{-2} , X_{CO} is dominated by dust shielding so that X_{CO} is lower at higher N_{H} , while at $N_{\text{H}} \gtrsim 10^{22}$ cm^{-2} , the CO emission is saturated by its large optical depth so that X_{CO} rises for higher N_{H} . In other words, the clouds with a typical column density of molecular clouds, $N_{\text{H}} \sim 10^{22}$ cm^{-2} , is the most efficient in CO emission per H_2 molecule around solar metallicity.

In Fig. 2b, we present the dependence on the UV radiation field intensity (χ). In the most intense radiation ($\chi = 170$), the H_2 fraction is strongly suppressed at a level where self-shielding is not important ($f_{\text{H}_2} < 2 \times 10^{-8}$ for $N_{\text{H}} = 10^{22}$ cm^{-2}) at $Z \lesssim 0.07 Z_{\odot}$; at higher metallicities, self-shielding coupled with the drastic increase of dust abundance makes the sharp transition toward the fully molecular phase in a narrow metallicity range of $0.007\text{--}0.2 Z_{\odot}$. The CO fraction is sensitive to χ at low metallicities where H_2 shielding is important, while it is less sensitive to χ at $Z \gtrsim 0.3 Z_{\odot}$, where dust shielding is important. This is because dust shielding, which has an exponential dependence on the dust-to-gas ratio, sufficiently suppresses the dissociating photons at high metallicity. Accordingly, the slope of X_{CO} as a function of Z changes in different χ . We will revisit this dependence on χ in Section 5.3.

3.3 Effects of the dust evolution parameters

We investigate the dependence on the parameters that regulate the dust evolution (Table 1). The resulting variation of the quantities of interest by the change of the parameters is shown in Fig. 3.

We show the effect of the dust condensation efficiency in stellar ejecta, f_{in} in Fig. 3a. As explained in H15, the stellar sources of dust dominate the dust-to-gas ratio at low metallicity before grain growth by accretion becomes efficient. Thus, the difference in \mathcal{D} between various f_{in} appears at $Z \lesssim 0.2 Z_{\odot}$. As a consequence, the effects of f_{in} on f_{H_2} and x_{CO} appear at low metallicity, where the CO abundance is too low for detection. Thus, the effect of f_{in} on x_{CO} and X_{CO} is difficult to be confirmed observationally. On the other hand, the effect of f_{in} on f_{H_2} could be examined if we observe objects with $Z \lesssim 0.2 Z_{\odot}$. A direct determination of H_2 abundance is possible for damped Lyman α objects (DLAs) using H_2 LW absorption lines (e.g. Ledoux et al. 2003).

In Fig. 3b, we show the dependence on β_{SN} , which regulates the efficiency of dust destruction by SNe. As expected, a stronger/weaker dust destruction decreases/increases both f_{H_2} and x_{CO} because of less/more shielding of dissociating photons. Around solar metallicity, since the CO abundance is governed by dust shielding, x_{CO} is almost inversely proportional to β_{SN} . However, X_{CO} does not vary as expected from the change of x_{CO} at solar metallicity, because the CO emission is optically thick.

In Fig. 3c, we present the dependence on τ_{cl} , which governs the efficiency of dust growth by accretion. This parameter determines the metallicity at which accretion significantly raise the dust-to-gas ratio (Hirashita & Kuo 2011). Accretion affects the H_2 abundance only if it occurs at low

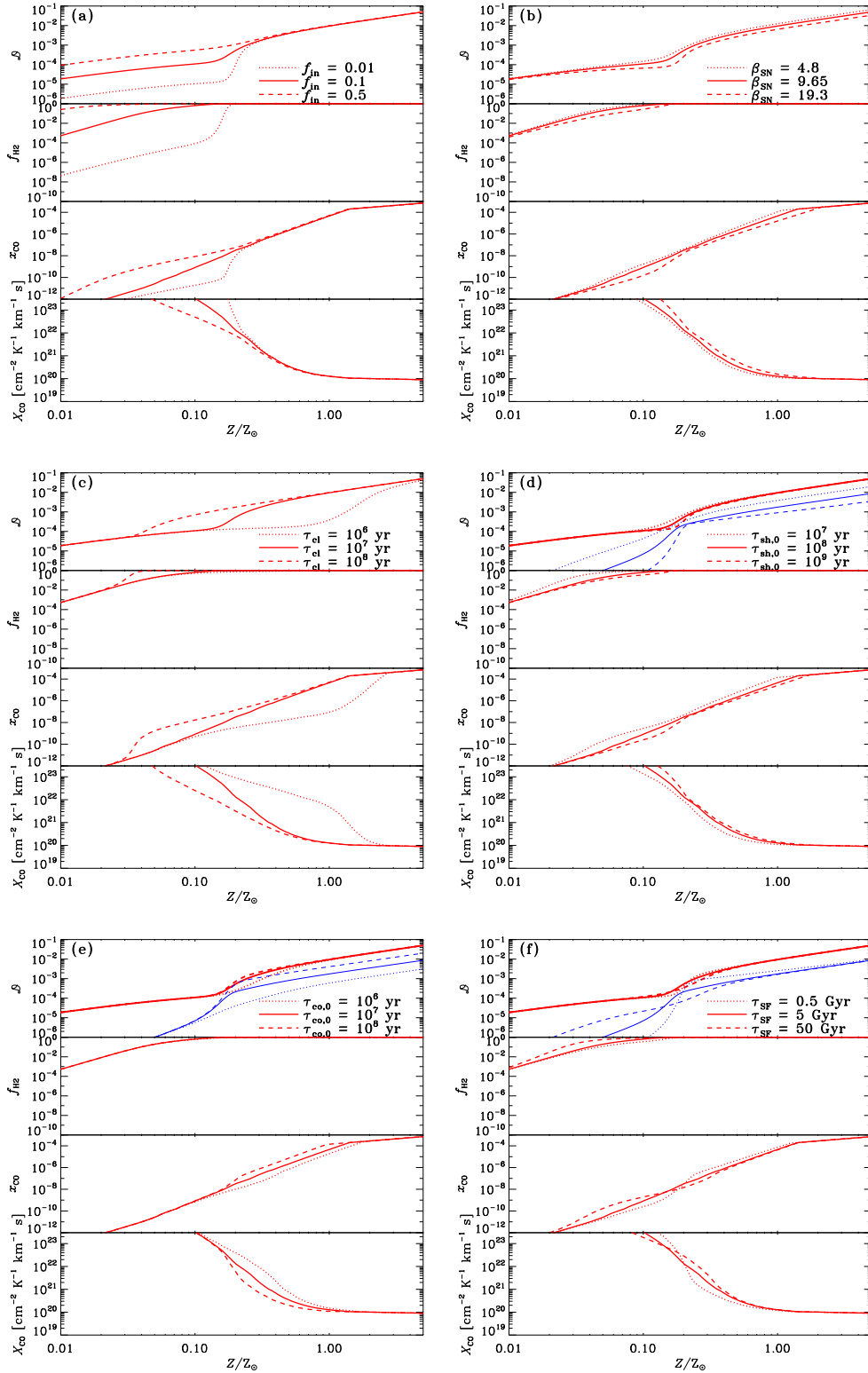


Figure 3. Same as Fig. 1 but with the following parameters changed: (a) $f_{\text{in}} = 0.01, 0.1,$ and 0.5 for the dotted, solid, and dashed lines, respectively. (b) $\beta_{\text{SN}} = 4.8, 9.65,$ and 19 for the dotted, solid, and dashed lines, respectively. (c) $\tau_{\text{cl}} = 10^6, 10^7,$ and 10^8 yr for the dotted, solid, and dashed lines, respectively. (d) $\tau_{\text{sh},0} = 10^7, 10^8,$ and 10^9 yr for the dotted, solid, and dashed lines, respectively. In the top window in this panel, we show the total dust-to-gas ratio (thick lines) and the small grain dust-to-gas ratio \mathcal{D}_s (thin lines), since the effect of shattering is clearly seen in the small-to-large grain abundance ratio. (e) $\tau_{\text{co},0} = 10^6, 10^7,$ and 10^8 yr for the dotted, solid, and dashed lines, respectively. In the top window of this panel, we show the total dust-to-gas ratio (thick lines) and the small grain dust-to-gas ratio \mathcal{D}_s (thin lines), since the effect of coagulation is clear in the small-to-large grain abundance ratio. (f) $\tau_{\text{SF}} = 0.5, 5,$ and 50 Gyr for the dotted, solid, and dashed lines, respectively. In the top window of this panel, we show the total dust-to-gas ratio (thick lines) and the small grain dust-to-gas ratio \mathcal{D}_s (thin lines). We fix the values of the parameters other than the varied parameter at the fiducial values listed in Table 1. We adopt the fiducial values for the parameters of the cloud in Table 2.

metallicity such as in the case of $\tau_{\text{cl}} = 10^8$ yr. Since the increase of CO abundance is associated with the increase of \mathcal{D} , accretion largely affects x_{CO} and X_{CO} . In particular, our results predict that the $X_{\text{CO}}-Z$ relation is sensitive to the metallicity level at which accretion dominates the increase of dust abundance. In the case of $\tau_{\text{cl}} = 10^6$ yr (the least efficient accretion), the effect of accretion only appears at super-solar metallicity; accordingly, x_{CO} remains low and X_{CO} is much higher than the Milky Way value ($\simeq 2 \times 10^{20}$ cm $^{-2}$ K $^{-1}$ km $^{-1}$ s) even at solar metallicity. In the case of $\tau_{\text{cl}} = 10^8$ yr (the most efficient accretion), in contrast, a high value of x_{CO} at low metallicity leads to a shallower slope in the $X_{\text{CO}}-Z$ relation than in the other cases. Thus, the $X_{\text{CO}}-Z$ relation depends largely on the efficiency of dust growth by accretion.

In Fig. 3d, we show the dependence on $\tau_{\text{sh},0}$, which regulates the efficiency of shattering (i.e. production of small grains from large grains). Small grains produced by shattering eventually grow by accretion. Thus, the increase of dust abundance by accretion appears at the lowest metallicity for the shortest $\tau_{\text{sh},0}$. In the top window of Fig. 3d, we also show the contribution from small grains to the dust-to-gas ratio: there is a clear difference in the small grain dust-to-gas ratio at all metallicities. Because small grains have a larger H $_2$ formation rate and dust extinction per dust mass than large grains, a larger fraction of small grains (or a higher efficiency of shattering) leads to a higher molecular abundance. Nevertheless, the effect of shattering on X_{CO} is minor compared with that of accretion.

In Fig. 3e, we show the dependence on the coagulation time-scale, $\tau_{\text{co},0}$. The effect of coagulation becomes prominent after the abundance of small grains has increased by shattering and accretion; thus, the variation of coagulation time-scale affects the quantities of interest only at $Z \gtrsim 0.1 Z_{\odot}$. Because the cloud becomes fully molecular at this metallicity, coagulation does not have any appreciable impact on the H $_2$ abundance. Since strong coagulation suppresses the abundance of small grains, it also suppresses accretion (recall that the role of accretion is to increase the small grain abundance; Section 2.1). As a result, the total dust abundance is the smallest in the case of the most efficient coagulation ($\tau_{\text{co},0} = 10^6$ yr) around $Z \sim 0.2-0.3 Z_{\odot}$. Moreover, coagulation also suppresses the relative abundance of small grains, which leads to a decrease of shielding effect (recall that small grains have larger dust optical depth per mass). As a consequence, the CO abundance is lower, and the CO-to-H $_2$ conversion factor is higher for a shorter $\tau_{\text{co},0}$.

In Fig. 3f, we examine the dependence on the star formation time-scale of the galaxy, τ_{SF} . The star formation time-scale regulates the time-scale of metal/dust enrichment by stellar sources. A quick metal enrichment leads to a quick increase in the large-grain abundance, while the time-scale of shattering is fixed so the production efficiency of small grains does not increase. Thus, the abundance of small grains relative to that of large grains is suppressed if τ_{SF} is short. Since small grains have larger shielding and H $_2$ formation rate per mass, the H $_2$ fraction is larger for a longer τ_{SF} . Because the shattering efficiency is higher if the abundance of large grains is higher, shattering, if it starts at a high metallicity (i.e. large \mathcal{D}_1) such as in the case of $\tau_{\text{SF}} = 0.5$ Gyr, has a dramatic impact on the increase in \mathcal{D} . Thus, the increase of

\mathcal{D}_s occurs in a narrow metallicity range for a short τ_{SF} . This produces a drastic change of x_{CO} and X_{CO} around $Z \sim 0.2-0.3 Z_{\odot}$. Therefore, the star formation time-scale also affects the metallicity dependence of CO abundance in such a way that mild star formation activities with long τ_{SF} tend to produce smooth increase (decrease) in x_{CO} (X_{CO}) as a function of metallicity.

4 DISCUSSION

4.1 Metallicity dependence of CO-to-H $_2$ conversion factor

The main purpose of this work is to clarify how the metallicity dependence of the H $_2$ and CO abundances is affected by the dust enrichment and evolution in galaxies. In particular, the CO-to-H $_2$ conversion factor has been measured for various types of galaxies with different metallicities. Indeed, it has been known observationally that the conversion factor depends strongly on metallicity. As shown above, the evolution of dust content, which regulates the abundances of H $_2$ and CO, is also driven by metallicity. For comparison with observations, we examine the relation between CO-to-H $_2$ conversion factor and metallicity.

We adopt the following data sets compiled in Bolatto et al. (2013). Leroy et al. (2011) estimated the CO-to-H $_2$ conversion factor in five Local Group galaxies using dust as a tracer of gas with a variation of dust-to-gas ratio among the galaxies taken into account. For their metallicity data given in the form of $12 + \log(\text{O}/\text{H})$, we put an uncertainty of 0.2, and assume that the solar metallicity corresponds to 8.7 following Bolatto et al. (2013) (we use the same oxygen abundance for the solar metallicity unless otherwise stated). For M31, M33, and the Small Magellanic Cloud, we adopt their spatially resolved data. Bolatto et al. (2008) derived the CO-to-H $_2$ conversion factor in nearby galaxies based on virial mass estimates of giant molecular clouds. We assume the same metallicity uncertainty (0.2) as assumed in the above sample. Israel (1997) estimated the CO-to-H $_2$ conversion factor in the Magellanic Clouds and nearby irregular galaxies. We also adopted their metallicity data. Sandstrom et al. (2013) analyzed spatially resolved CO, dust, and H I maps on \sim kpc scales of nearby star-forming galaxies, and derived the spatially resolved CO-to-H $_2$ conversion factor. We adopt their mean CO-to-H $_2$ conversion factor for each galaxy. We take the metallicity data of their sample from Moustakas et al. (2010): among their metallicity calibrations, we adopt the one by Pilyugin & Thuan (2005) and assume, following Bolatto et al. (2013), that the solar metallicity corresponds to $12 + \log(\text{O}/\text{H}) = 8.5$. Besides, we newly add the data taken from Cormier et al. (2014) for nearby low-metallicity galaxies. They obtained X_{CO} , assuming dust to trace the molecular gas with a variation dust-to-gas ratio among galaxies taken into account.

There are two remarks on the observationally derived CO-to-H $_2$ conversion factors. The dust-based X_{CO} estimates (i.e. other than Bolatto et al. 2008 above) commonly assume that the dust-to-gas ratio in molecular clouds is the same as that in diffuse gas. In reality, we expect that the dust-to-gas ratio in molecular clouds is higher because of dust

growth. If this is true, the dust-based X_{CO} estimate adopts an underestimated dust-to-gas ratio. A lower dust-to-gas ratio would overestimate the molecular gas mass by a factor of ~ 2 (Leroy et al. 2011), which leads to overestimation of X_{CO} in the observational data. Since we consider a large dynamic range for X_{CO} and there is an order-of-magnitude scatter in the observational data, a factor 2 difference in dust-to-gas ratio would not affect the overall comparison shown in this section. Our theoretical model also does not distinguish between dust components in molecular clouds and in diffuse gas, which leads to underestimation of the dust-to-gas ratio (i.e. underestimation of the shielding effect of dissociating photons) in molecular clouds, and thus, overestimation of X_{CO} in our theoretical models. Thus, if we could consider the difference between the dust-to-gas ratios between dense and diffuse gas, both theoretical predictions and observational data of X_{CO} would move in the same direction; thus, it is not clear if the comparison is drastically affected by dust growth in molecular clouds. In fact, dust growth could already occur in the diffuse (but relatively dense) ISM as shown in the numerical simulation by Zhukovska et al. (2016). Thus, to fully address the effect of dust growth on X_{CO} estimate, we need to use a simulation that includes consistently the evolution of the ISM and that of dust (Aoyama et al. 2016), and need to include molecule formation and destruction consistently with the simulation. Such a complete framework is left for future work.

The other remark is that the virial-mass-based X_{CO} estimate (i.e. Bolatto et al. 2008 above) may not be sensitive to CO-dark layers in molecular clouds. However, we do not find any offset in the $X_{\text{CO}}-Z$ relation between Bolatto et al. (2008)'s sample and the other samples; thus, we simply include all the above data in the same diagram, although we should keep in mind the inhomogeneity in the method of deriving X_{CO} . There is another way of observationally deriving X_{CO} : Amorín et al. (2016) derived the molecular gas mass by assuming a star formation law. The CO-to- H_2 conversion factors they derived are consistent with (or within the scatter of) the ones based on direct gas mass tracers (i.e. the data plotted in Fig. 4). We should also note that some galaxies appear for multiple times and that we did not make any effort of unifying them into a single data point. However, the difference among the metallicities of the same galaxy is within 0.2 dex, which is smaller than the scatter in the $X_{\text{CO}}-Z$ diagram. Moreover, the scatter of X_{CO} caused by the multiplicity is smaller than the difference between different galaxies at a similar metallicity; thus, the multiplicity does not affect our results.

In Fig. 4, we show the comparison of our results with the observational data for the $X_{\text{CO}}-Z$ relation. We also compare the $\mathcal{D}-Z$ relations with nearby galaxy data taken from Rémy-Ruyer et al. (2014). In deriving the dust-to-gas ratio, they estimated the gas mass by the sum of atomic and molecular gas mass. For the molecular gas mass, they examined both the Milky Way and the metallicity-dependent CO-to- H_2 conversion factors. Strictly speaking we need to assume a consistent conversion factor with the one predicted by our model, but they showed that the difference in the conversion factor only changes the dust-to-gas ratio within the scatter of the observational data. Thus, we simply adopt their dust-to-gas ratios based on the Milky Way conversion factor. The $\mathcal{D}-Z$ relations predicted by our models are broadly consis-

tent with the data as already discussed in H15. Our theoretical predictions are also consistent with the $X_{\text{CO}}-Z$ relation plotted in the figure. In general, the scatter of observational data is too large to constrain most of the parameters in the models. Nevertheless, inefficient accretion represented by $\tau_{\text{cl}} = 10^6$ yr can be rejected (see Fig. 4c), since it predicts too high conversion factors. In this case, the dust-to-gas ratio is so low that shielding of dissociating photons is not enough to realize a high CO abundance (see also Fig. 3c). Such a low accretion efficiency also tends to underproduce the observed dust-to-gas ratio as a function of metallicity as shown in the upper window of Fig. 4c.

As mentioned above, the scatter of the observational data is much larger than the variation of the $X_{\text{CO}}-Z$ relations predicted by the models if the parameters other than τ_{cl} are changed. The dust condensation efficiency in stellar ejecta (f_{in}) has a large impact at low metallicities, where CO is difficult to detect. Yet, it is interesting to note that Cormier et al. (2014)'s lowest metallicity data lie in the range where the difference in X_{CO} among various values of f_{in} can be seen. At the metallicity range where a statistical number of data for X_{CO} are available, interstellar processing is more important than stellar dust production. As concluded by our previous work (H15) as well as by many other studies (Dwek 1998; Hirashita 1999; Inoue 2003; Zhukovska et al. 2008; Hirashita & Kuo 2011; Valiante et al. 2011; Mattsson & Andersen 2012; Kuo et al. 2013; de Bennassuti et al. 2014; Michałowski 2015; Mancini et al. 2015; Schneider et al. 2016; Popping et al. 2016), dust growth by accretion is the major driver of the evolution of dust-to-gas ratio at $Z \gtrsim 0.1 Z_{\odot}$ (see Rouillé et al. 2014 for experimental evidence; but see Ferrara et al. 2016). In conclusion, dust growth by accretion not only drives the evolution of dust-to-gas ratio but also have a significant impact on the relation between X_{CO} and metallicity. The other processes than accretion have minor impacts on the $X_{\text{CO}}-Z$ relation.

4.2 Effects of grain size distribution

One of the unique features in our modeling is the capability to calculate the grain size distribution in the form of the mass ratio between small and large grains. The effects of grain size distribution appear directly in H_2 formation (equation 6) and shielding (dust extinction) (equation 12). We here examine how the grain size distribution affects these processes.

4.2.1 Effects on H_2 formation

In order to investigate the effect of grain size distribution on H_2 formation, we take the following two extremes. One is that we adopt the H_2 formation rate on small grains for both large and small grains in equation (6); that is, all the grains are assumed to be small grains when we estimate the H_2 formation rate. The other is the opposite; that is, we adopt the H_2 formation rate of large grains for both large and small grains. The former extreme represents the highest H_2 formation efficiency (referred to as the high H_2 formation rate), while the latter shows the lowest efficiency (referred to as the low H_2 formation rate). We also show the H_2 formation

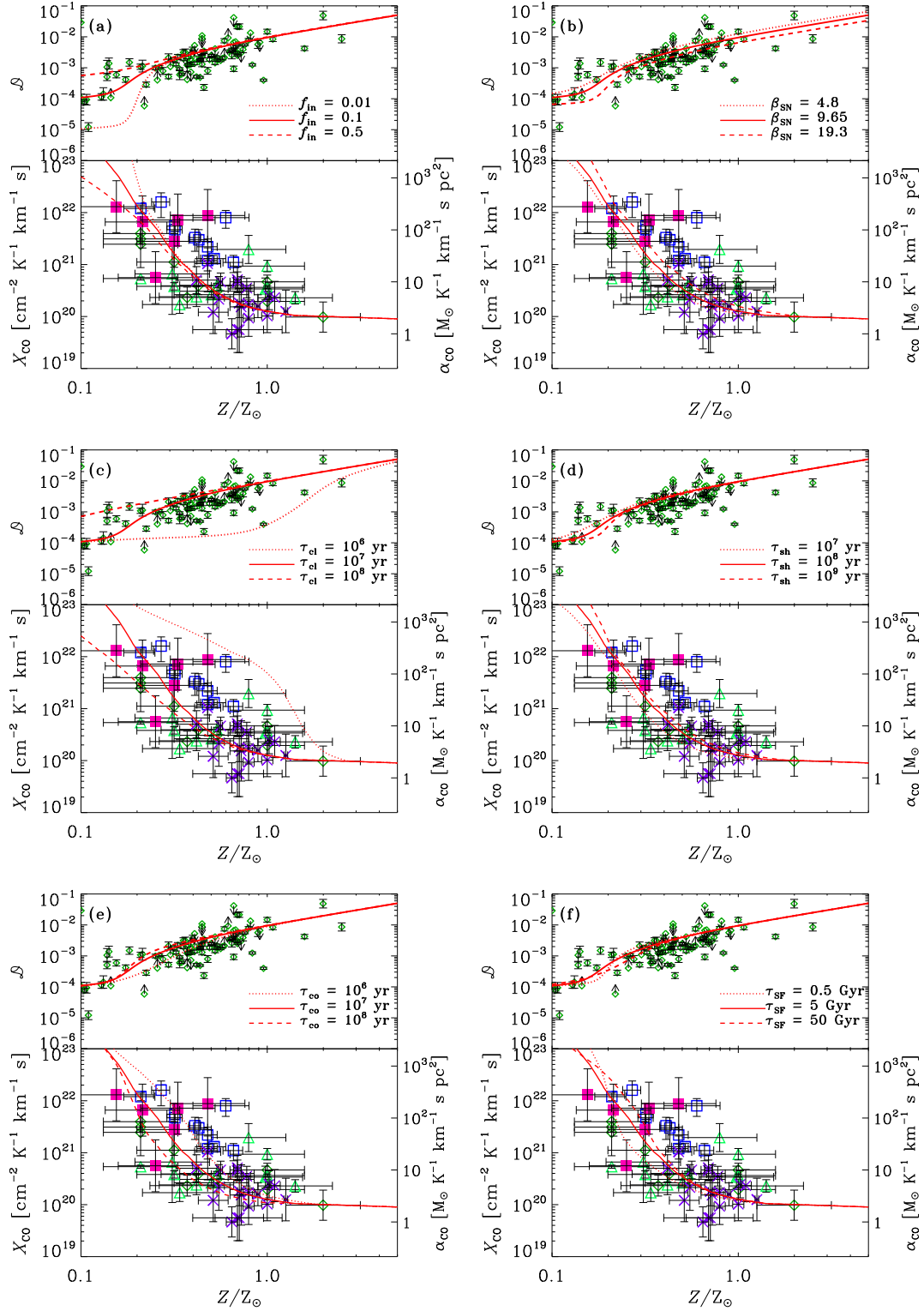


Figure 4. Upper window in each panel: Relation between dust-to-gas ratio and metallicity. Lower window in each panel: Metallicity dependence of CO-to-H₂ conversion factor. The two definitions of the conversion factor are shown on the left and right vertical axes. The models in Panels (a)–(f) are the same as those shown in the top and bottom windows of Figs. 3(a)–(f), respectively. The parameters adopted for the lines in each panel are the same as those in Fig. 3, and are also indicated in the panels. We fix the values of the parameters other than the varied parameter at the fiducial values listed in Table 1. We adopt the fiducial values for the parameters of the cloud in Table 2. The points with error bars show the observation data: the data in the upper windows are taken from Rémy-Ruyer et al. (2014) and those in the lower windows from Leroy et al. (2011) (diamonds), Bolatto et al. (2008) (triangles), Israel (1997) (open squares), Sandstrom et al. (2013) (crosses), and Cormier et al. (2014) (filled squares). See Section 4.1 for more detailed descriptions of the data.

rate in our models (consistent with the evolution of grain size distribution), which is referred to as the standard H₂ formation rate. We use the fiducial values for the parameters (Tables 1 and 2) unless otherwise stated.

In Fig. 5a, we show the evolution of the quantities of interest as a function of metallicity for the high and low H₂ formation rates, in comparison with the standard H₂ formation rate. The high H₂ formation rate predicts that the cloud becomes almost fully molecular in the metallicity range $Z \gtrsim 0.01 Z_{\odot}$. The low H₂ formation rate shows a similar evolution to the case of the standard H₂ formation rate, since the dust abundance is dominated by large grains in the low-metallicity phase of galaxy evolution. The difference between these two cases become visible around $Z \sim 0.1 Z_{\odot}$ because of the small grain production by shattering and accretion. Thus, the enhancement of H₂ formation rate by these small grain production mechanisms is important for the H₂ abundance at such a low metallicity as $Z \sim 0.1 Z_{\odot}$. At higher metallicities, hydrogen becomes fully molecular, and the effect of H₂ formation rate is not important. The CO abundance is also affected by different grain sizes at low metallicities because of the difference in H₂ shielding of dissociating photons. However, the CO-to-H₂ conversion factor does not change significantly by the variation of grain sizes in the metallicity range where detection of CO is possible ($Z \gtrsim 0.1 Z_{\odot}$).

As shown in Fig. 2, the radiation field affects the H₂ abundance drastically. Thus, we investigate the effects of grain-size-dependent H₂ formation rate for the strongest radiation field $\chi = 170$ in Fig. 5b. The same behaviour for f_{H_2} as seen for $\chi = 1.7$ (the fiducial value) is observed, but with an enhanced difference among the three cases for the H₂ formation rate. In particular, the H₂ fraction is completely different at $Z \sim 0.1\text{--}0.2 Z_{\odot}$. However, at higher metallicities, the gas is fully molecular in any case; thus, the CO abundance and CO-to-H₂ conversion factor are unaffected at $Z \gtrsim 0.2 Z_{\odot}$.

In summary, the effect of grain size distribution on H₂ formation rate is important at low metallicities (typically $Z \lesssim 0.2 Z_{\odot}$). Thus, if we interpret the H₂ abundance in low-metallicity systems such as DLAs (Lanzetta et al. 1989; Ledoux et al. 2003) and nearby dwarf galaxies (Kamaya & Hirashita 2001), the effect of grain size distribution is important, especially for environments with intense UV radiation field. However, even in the intense UV field, hydrogen becomes fully molecular at high metallicities ($Z \gtrsim 0.3 Z_{\odot}$). Consequently, the CO-to-H₂ conversion factor is not affected by the dependence of H₂ formation rate on the grain size distribution at $Z \gtrsim 0.3 Z_{\odot}$.

4.2.2 Effects on dust shielding

The grain size distribution also influences dust shielding of dissociating photons. As formulated in equations (11) and (12), small grains have larger efficiencies of shielding than large grains. We take the two extremes: in one case we adopt the optical depth for small grains for both large and small grains in equation (12); that is, all the grains are assumed to be small when we estimate the optical depth for dissociating photons. This case is referred to as the high extinction. The other is the opposite: we adopt the optical depth for dissociating photons by assuming that all the grains are large

grains. This case is referred to as the low extinction. The calculation consistent with the grain size evolution is referred to as the standard extinction. We use the fiducial values for the parameters (Tables 1 and 2) unless otherwise stated.

In Fig. 6a, we show the quantities of interest as a function of metallicity for the high and low extinctions of dissociating photons in comparison with the standard case. The change of extinction does not largely affect the H₂ fraction since self-shielding is more important. The effect of extinction is rather important for the CO fraction and the CO-to-H₂ conversion factor. In contrast to the effect of grain size on H₂ formation, dust shielding affects the CO abundance also at high metallicity.

We also investigate a case with high radiation field $\chi = 170$ in Fig. 6b. Comparing f_{H_2} in Figs. 5b and 6b, we observe that the effect of grain size on dust shielding is less important for f_{H_2} than that on H₂ formation. On the other hand, dust shielding is again important for the CO abundance; in particular, the metallicity dependence of the CO-to-H₂ conversion factor at sub-solar metallicity is driven more by dust shielding than by H₂ shielding. This is why the conversion factor is affected by coagulation and shattering (i.e. main mechanisms of changing the grain size distribution) as shown in Fig. 4.

5 OBSERVATIONAL IMPLICATIONS

5.1 Uncertainty in molecular mass estimates

The variation of CO-to-H₂ conversion factor among galaxies can be produced by the different dust evolution histories. In particular, we have shown that if the efficiency of dust growth by accretion varies, the $X_{\text{CO}}\text{--}Z$ relation is significantly perturbed. This causes an uncertainty in molecular mass estimates, since we do not know the efficiency of dust growth *a priori* in observing a galaxy. Note that this uncertainty still remains even if we know the metallicity.

The molecular gas mass is often related to the star formation rate. It has been known that there is a good correlation between these two quantities. The correlation – the so-called star formation law – has been extensively discussed in various contexts (e.g. Leroy et al. 2013). The above uncertainty caused by the dust evolution history contributes to the scatter of the observationally derived H₂ mass from CO luminosity. In particular, if a sample contains objects with a variety of metallicities, the effect of dust evolution, especially dust growth by accretion, should be carefully discussed, since it may cause a significant scatter in the $X_{\text{CO}}\text{--}Z$ relation as shown in Fig. 4c.

5.2 Nearby low-metallicity galaxies

As expected from the above results, low-metallicity galaxies are indeed deficient in CO (e.g. Schrubba et al. 2012), and large part of carbon atoms are rather traced by [C II] emission (Madden et al. 1997; Cormier et al. 2014). According to our calculations above, hydrogen in a cloud whose column density is typical of molecular clouds in the local Universe ($N_{\text{H}} \sim 10^{22} \text{ cm}^{-2}$) becomes fully molecular around $Z \sim 0.1 Z_{\odot}$, while the CO-to-H₂ conversion factor is still an order of magnitude larger than the Milky Way value around $Z \sim 0.4$

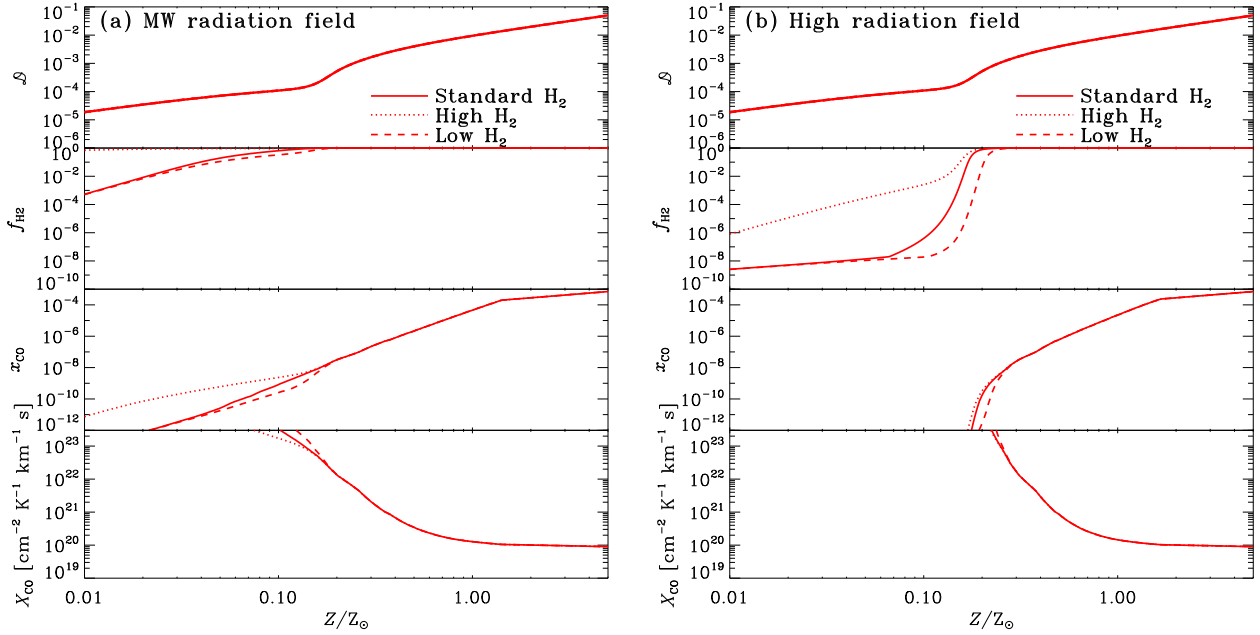


Figure 5. Same as Fig. 1 but for high and low H_2 formation rates, for the dotted and dashed lines, respectively. For the high (low) H_2 formation rate, we assume that all the grains are small (large) grains. Panels (a) and (b) adopt $\chi = 1.7$ (the Milky Way radiation field) and 170, respectively, with the other parameters fixed to the fiducial values (Tables 1 and 2).

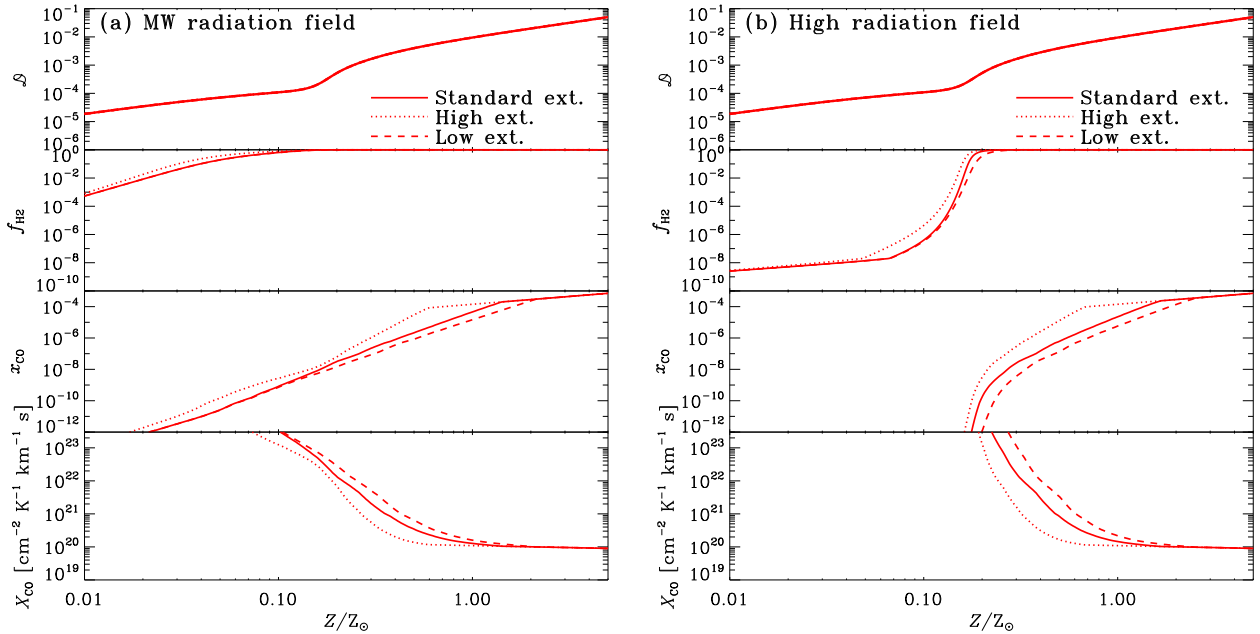


Figure 6. Same as Fig. 1 but for high and low dust extinctions of dissociating photons, for the dotted and dashed lines, respectively. For the high (low) extinctions, we assume that all the grains are small (large) grains. Panels (a) and (b) adopt $\chi = 1.7$ (the Milky Way radiation field) and 170, respectively, with the other parameters fixed to the fiducial values (Tables 1 and 2).

Z_\odot in our fiducial case. Thus, we expect that such a fully molecular gas is difficult to be traced by CO around ~ 0.1 – $0.4 Z_\odot$, which just corresponds to metallicities in nearby low-metallicity dwarf galaxies. Recently, it has also been suggested that [C I] is a better tracer of molecular gas at low

metallicity than CO (Glover & Clark 2016). At $Z < 0.1 Z_\odot$, a cloud with $N_H \sim 10^{22} \text{ cm}^{-2}$ is not fully molecular. Thus, it is expected that H I gas rather than molecular gas becomes relatively important for the total gas content.

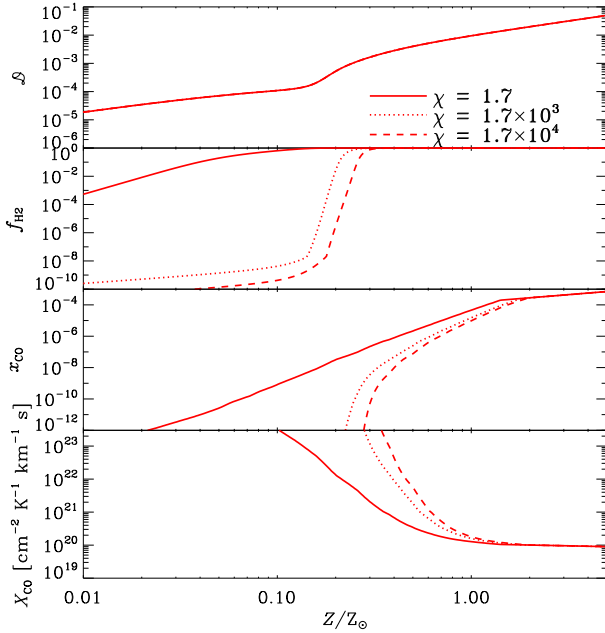


Figure 7. Same as Fig. 1 but for extremely high values for χ (1.7×10^3 and 1.7×10^4 ; dotted and dashed lines) appropriate for starburst galaxies. We also show the fiducial value (Milky Way value) $\chi = 1.7$ (solid line) as a reference. The other parameters are fixed to the fiducial values (Tables 1 and 2).

5.3 Starburst galaxies

Some observations have suggested that starburst galaxies such as (ultra)luminous infrared galaxies [(U)LIRGs] have CO-to-H₂ conversion factors $X_{\text{CO}} \sim 0.2\text{--}1 \times 10^{20} \text{ cm}^{-2} \text{ K}^{-1} \text{ km}^{-1} \text{ s}$, which are lower than the conversion factor in the Milky Way by a factor of 2–10 (see section 7 of Bolatto et al. 2013, for a review). As argued in Section 2.5, they have 10–100 times higher surface SFR density than nearby disc galaxies; thus, we first calculate the metallicity dependence of the quantities of interest with $\chi = 1.7 \times 10^3$ and 1.7×10^4 . The results for these high radiation field intensities are shown in Fig. 7. As expected, the H₂ and CO abundances are suppressed under such a high radiation field. However, the cloud still becomes fully molecular at $Z \gtrsim 0.3 Z_{\odot}$. The metallicity dependence of X_{CO} is steeper for a higher χ , but X_{CO} is insensitive to χ around solar metallicity. This is because dust shielding creates a favourable condition for the CO formation around solar metallicity even if the radiation field is four orders of magnitude higher than the Galactic value. Moreover, the CO $J = 1\text{--}0$ line is optically thick at high metallicity (i.e. the metallicity dependence of X_{CO} is very weak). Thus, the observed systematically lower conversion factors in starburst galaxies should be interpreted not by metallicity dependence or a stronger radiation field intensity but by a change of other physical conditions. In fact, the low conversion factors in starburst galaxies could be explained by high gas temperatures (Wild et al. 1992) or high velocity dispersions (Zhu et al. 2003; Papadopoulos et al. 2012) or both (Narayanan et al. 2011).

5.4 High- z galaxies

Tacconi et al. (2008) studied submillimetre galaxies (SMGs) and UV/optically selected galaxies at $z \sim 2$ and found that they have similar CO-to-H₂ conversion factors to those found in nearby (U)LIRGs. Daddi et al. (2010) showed that the so-called main-sequence galaxies at $z \sim 1.5$ have conversion factors similar to the Milky Way ones. The difference in the conversion factor between SMGs and main-sequence galaxies is also found by Magdis et al. (2011). Magnelli et al. (2012) show that there is a correlation between CO-to-H₂ conversion factor and dust temperature for galaxies at $z \sim 1$. Although this dust temperature dependence of X_{CO} could be interpreted as an effect of the radiation field, we have shown above that the difference in χ , as shown in Fig. 2, does not produce a large difference in the conversion factor around solar metallicity appropriate for their sample. It should be due to effects not explicitly included in our paper such as high gas temperatures and large velocity dispersions.

Studies on metallicity dependence of CO-to-H₂ conversion factor have been made possible also at $z \gtrsim 1$. Genzel et al. (2012) used a sample of main-sequence galaxies and found a similar metallicity dependence of X_{CO} to that seen for nearby galaxies. This indicates that our models, which explain the $X_{\text{CO}}\text{--}Z$ relation in nearby galaxies, can also be applicable to high-redshift galaxies. Since dust growth by accretion has a strong influence on the $X_{\text{CO}}\text{--}Z$ relation at a range of Z appropriate for CO detection (i.e. $Z \gtrsim 0.1 Z_{\odot}$), their result implies that galaxies at $z \gtrsim 1$ have similar efficiencies of dust growth by accretion to those in nearby galaxies.

6 CONCLUSION

We investigate the effect of dust evolution on the metallicity dependence of CO-to-H₂ conversion factor (X_{CO}). To this aim, we first need to understand the dependence of dust abundance on metallicity, since dust affects the molecular abundances through H₂ formation on dust surface and shielding of dissociating photons. The dust abundance as a function of metallicity is modeled by including all major processes driving the dust evolution: dust condensation in stellar ejecta, dust destruction in SN shocks, grain growth by accretion and coagulation, and grain disruption by shattering. The grain size distribution is represented by the small-to-large grain abundance ratio, which is consistently treated with the dust evolution. The relation between dust-to-gas ratio and metallicity ($\mathcal{D}\text{--}Z$ relation) is used to calculate the H₂ fraction and CO abundance in a cloud with $N_{\text{H}} \sim 10^{22} \text{ cm}^{-2}$ as a function of metallicity by considering dust shielding of dissociating photons and H₂ formation on dust surface under given interstellar radiation field and hydrogen column density. The effects of grain size on H₂ formation and shielding are also included. The major output of our model is the CO-to-H₂ conversion factor, X_{CO} .

As a consequence of the modeling, we predict consistent metallicity dependence of X_{CO} ($X_{\text{CO}}\text{--}Z$ relation) with observational data. Among various processes driving dust evolution, grain growth by accretion has the largest impact on the $X_{\text{CO}}\text{--}Z$ relation. Efficient accretion, which is also needed to reproduce the $\mathcal{D}\text{--}Z$ relation of nearby galaxies, is strongly

required to explain the $X_{\text{CO}}-Z$ relation. The dust condensation efficiency in stellar ejecta also affects X_{CO} , but the effect appears at low metallicity ($\lesssim 0.2 Z_{\odot}$), where detection of CO is difficult. The other processes also have some impacts on X_{CO} , but the effects are minor compared with the scatter of the observational data at the metallicity range ($Z \gtrsim 0.1 Z_{\odot}$) where CO could be detected.

We also find that dust condensation in stellar ejecta has a dramatic impact on the H_2 abundance at low metallicities ($\lesssim 0.1 Z_{\odot}$) and that the grain size dependence of H_2 formation rate is also important. Such a metallicity range is relevant for damped Lyman α systems and extremely low-metallicity dwarf galaxies. Between ~ 0.1 and $\sim 0.4 Z_{\odot}$, although clouds with a typical column density of ‘molecular clouds’ ($N_{\text{H}} \sim 10^{22} \text{ cm}^{-2}$) become fully molecular ($f_{\text{H}_2} \sim 1$), X_{CO} is more than two orders of magnitude larger than the Milky Way value; thus, molecular clouds are CO-dark in this metallicity range. Applicability of our models to the $X_{\text{CO}}-Z$ relation of $z \gtrsim 1$ main-sequence galaxies implies that their dominant mechanism of dust abundance evolution is similar to that in nearby galaxies.

ACKNOWLEDGEMENTS

We are grateful to A. Rémy-Ruyer for providing us with the data for the relation between dust-to-gas ratio and metallicity of nearby galaxies. HH thanks A. Ferrara, D. Cormier, R. Feldmann, and A. D. Bolatto for extremely useful discussions and comments and the staff at Kavli Institute for Theoretical Physics, University of California, Santa Barbara for their hospitality during the program ‘the Cold Universe’. We also thank the anonymous referee for useful comments. This research was supported in part by the National Science Foundation under Grant No. NSF PHY11-25915. HH is supported by the Ministry of Science and Technology grant MOST 105-2112-M-001-027-MY3.

REFERENCES

- Amorín R., Muñoz-Tuñón C., Aguerri J. A. L., Planesas P., 2016, *A&A*, **588**, A23
- Aoyama S., Hou K.-C., Shimizu I., Hirashita H., Todoroki K., Choi J.-H., Nagamine K., 2016, preprint, ([arXiv:1609.07547](https://arxiv.org/abs/1609.07547))
- Arimoto N., Sofue Y., Tsujimoto T., 1996, *PASJ*, **48**, 275
- Asano R. S., Takeuchi T. T., Hirashita H., Nozawa T., 2013, *MNRAS*, **432**, 637
- Asano R. S., Takeuchi T. T., Hirashita H., Nozawa T., 2014, *MNRAS*, **440**, 134
- Bekki K., 2015, *MNRAS*, **449**, 1625
- Bekki K., Hirashita H., Tsujimoto T., 2015, *ApJ*, **810**, 39
- Bolatto A. D., Leroy A. K., Rosolowsky E., Walter F., Blitz L., 2008, *ApJ*, **686**, 948
- Bolatto A. D., Wolfire M., Leroy A. K., 2013, *ARA&A*, **51**, 207
- Cazaux S., Tielens A. G. G. M., 2004, *ApJ*, **604**, 222
- Cormier D., et al., 2014, *A&A*, **564**, A121
- Daddi E., et al., 2010, *ApJ*, **713**, 686
- de Bressan M., Schneider R., Valiante R., Salvadori S., 2014, *MNRAS*, **445**, 3039
- Draine B. T., 1978, *ApJS*, **36**, 595
- Draine B. T., Bertoldi F., 1996, *ApJ*, **468**, 269
- Draine B. T., Lee H. M., 1984, *ApJ*, **285**, 89
- Dwek E., 1998, *ApJ*, **501**, 643
- Feldmann R., Gnedin N. Y., Kravtsov A. V., 2012, *ApJ*, **747**, 124
- Ferrara A., Viti S., Ceccarelli C., 2016, *MNRAS*, **463**, L112
- Gallerani S., et al., 2010, *A&A*, **523**, A85
- Genzel R., et al., 2012, *ApJ*, **746**, 69
- Gibson S. J., et al., 2015, preprint, ([arXiv:1510.06784](https://arxiv.org/abs/1510.06784))
- Glover S. C. O., Clark P. C., 2016, *MNRAS*, **456**, 3596
- Glover S. C. O., Mac Low M.-M., 2011, *MNRAS*, **412**, 337
- Glover S. C. O., Federrath C., Mac Low M.-M., Klessen R. S., 2010, *MNRAS*, **404**, 2
- Gould R. J., Salpeter E. E., 1963, *ApJ*, **138**, 393
- Habing H. J., 1968, *Bull. Astron. Inst. Netherlands*, **19**, 421
- Hirashita H., 1999, *ApJ*, **510**, L99
- Hirashita H., 2015, *MNRAS*, **447**, 2937
- Hirashita H., Ferrara A., 2005, *MNRAS*, **356**, 1529
- Hirashita H., Kuo T.-M., 2011, *MNRAS*, **416**, 1340
- Hollenbach D., McKee C. F., 1979, *ApJS*, **41**, 555
- Hou K.-C., Hirashita H., Michałowski M. J., 2016, *PASJ*, **68**, 94
- Hu C.-Y., Naab T., Walch S., Glover S. C. O., Clark P. C., 2016, *MNRAS*, **458**, 3528
- Hunt L. K., et al., 2015, *A&A*, **583**, A114
- Inoue A. K., 2003, *PASJ*, **55**, 901
- Israel F. P., 1997, *A&A*, **328**, 471
- Kamaya H., Hirashita H., 2001, *PASJ*, **53**, 483
- Kennicutt Jr. R. C., 1998, *ApJ*, **498**, 541
- Krumholz M. R., McKee C. F., Tumlinson J., 2008, *ApJ*, **689**, 865
- Krumholz M. R., McKee C. F., Tumlinson J., 2009, *ApJ*, **693**, 216
- Kuo T.-M., Hirashita H., Zafar T., 2013, *MNRAS*, **436**, 1238
- Lanzetta K. M., Wolfe A. M., Turnshek D. A., 1989, *ApJ*, **344**, 277
- Ledoux C., Petitjean P., Srianand R., 2003, *MNRAS*, **346**, 209
- Lee H.-H., Herbst E., Pineau des Forets G., Roueff E., Le Bourlot J., 1996, *A&A*, **311**, 690
- Leroy A. K., et al., 2011, *ApJ*, **737**, 12
- Leroy A. K., et al., 2013, *AJ*, **146**, 19
- Lisenfeld U., Ferrara A., 1998, *ApJ*, **496**, 145
- Madden S. C., Poglitsch A., Geis N., Stacey G. J., Townes C. H., 1997, *ApJ*, **483**, 200
- Magdis G. E., et al., 2011, *ApJ*, **740**, L15
- Magnelli B., et al., 2012, *A&A*, **548**, A22
- Maiolino R., Schneider R., Oliva E., Bianchi S., Ferrara A., Mannucci F., Pedani M., Roca Sogorb M., 2004, *Nature*, **431**, 533
- Maloney P., Black J. H., 1988, *ApJ*, **325**, 389
- Mancini M., Schneider R., Graziani L., Valiante R., Dayal P., Maio U., Ciardi B., Hunt L. K., 2015, *MNRAS*, **451**, L70
- Mattsson L., Andersen A. C., 2012, *MNRAS*, **423**, 38
- McKee C. F., Krumholz M. R., 2010, *ApJ*, **709**, 308
- McKinnon R., Torrey P., Vogelsberger M., 2016, *MNRAS*, **457**, 3775
- Michałowski M. J., 2015, *A&A*, **577**, A80
- Moustakas J., Kennicutt Jr. R. C., Tremonti C. A., Dale D. A., Smith J.-D. T., Calzetti D., 2010, *ApJS*, **190**, 233
- Narayanan D., Krumholz M., Ostriker E. C., Hernquist L., 2011, *MNRAS*, **418**, 664
- Narayanan D., Krumholz M. R., Ostriker E. C., Hernquist L., 2012, *MNRAS*, **421**, 3127
- Naslim N., et al., 2015, *MNRAS*, **446**, 2490
- Nozawa T., Asano R. S., Hirashita H., Takeuchi T. T., 2015, *MNRAS*, **447**, L16
- Omukai K., Tsuribe T., Schneider R., Ferrara A., 2005, *ApJ*, **626**, 627
- Papadopoulos P. P., van der Werf P., Xilouris E., Isaak K. G., Gao Y., 2012, *ApJ*, **751**, 10
- Pei Y. C., 1992, *ApJ*, **395**, 130
- Pilyugin L. S., Thuan T. X., 2005, *ApJ*, **631**, 231
- Popping G., Somerville R. S., Galametz M., 2016, preprint, ([arXiv:1609.08622](https://arxiv.org/abs/1609.08622))
- Rémy-Ruyer A., et al., 2014, *A&A*, **563**, A31
- Rouillé G., Jäger C., Krasnokutski S. A., Krebsz M., Henning T., 2014, *Faraday Discuss.*, **168**, 449

- Sandstrom K. M., et al., 2013, *ApJ*, **777**, 5
- Schaerer D., 2002, *A&A*, **382**, 28
- Schaerer D., Boone F., Zamojski M., Staguhn J., Dessauges-Zavadsky M., Finkelstein S., Combes F., 2015, *A&A*, **574**, A19
- Schneider R., Omukai K., Inoue A. K., Ferrara A., 2006, *MNRAS*, **369**, 1437
- Schneider R., Hunt L., Valiante R., 2016, *MNRAS*, **457**, 1842
- Schruba A., et al., 2012, *AJ*, **143**, 138
- Shetty R., Glover S. C., Dullemond C. P., Ostriker E. C., Harris A. I., Klessen R. S., 2011, *MNRAS*, **415**, 3253
- Spitzer L., 1978, *Physical Processes in the Interstellar Medium*. Wiley, New York
- Tacconi L. J., et al., 2008, *ApJ*, **680**, 246
- Tchernyshyov K., Meixner M., Seale J., Fox A., Friedman S. D., Dwek E., Galliano F., 2015, *ApJ*, **811**, 78
- Tielens A. G. G. M., 2005, *The Physics and Chemistry of the Interstellar Medium*. Cambridge University Press, Cambridge
- Tinsley B. M., 1980, *Fundamentals Cosmic Phys.*, **5**, 287
- Valiante R., Schneider R., Bianchi S., Andersen A. C., 2009, *MNRAS*, **397**, 1661
- Valiante R., Schneider R., Salvadori S., Bianchi S., 2011, *MNRAS*, **416**, 1916
- Ward-Thompson D., André P., Crutcher R., Johnstone D., Onishi T., Wilson C., 2007, *Protostars and Planets V*, pp 33–46
- Weingartner J. C., Draine B. T., 2001, *ApJ*, **548**, 296
- Wild W., Harris A. I., Eckart A., Genzel R., Graf U. U., Jackson J. M., Russell A. P. G., Stutzki J., 1992, *A&A*, **265**, 447
- Wilson C. D., 1995, *ApJ*, **448**, L97
- Yajima H., Nagamine K., Thompson R., Choi J.-H., 2014, *MNRAS*, **439**, 3073
- Yamasawa D., Habe A., Kozasa T., Nozawa T., Hirashita H., Umeda H., Nomoto K., 2011, *ApJ*, **735**, 44
- Yan H., Lazarian A., Draine B. T., 2004, *ApJ*, **616**, 895
- Zhu M., Seaquist E. R., Kuno N., 2003, *ApJ*, **588**, 243
- Zhukovska S., Gail H.-P., Tieloff M., 2008, *A&A*, **479**, 453
- Zhukovska S., Dobbs C., Jenkins E. B., Klessen R. S., 2016, *ApJ*, **831**, 147

APPENDIX A: ASSUMED GRAIN SIZE DISTRIBUTION AND MOMENTS

In the two-size approximation, we simply represent the grain sizes with large and small grains. However, in order to predict statistical properties, it is necessary to *assume* a functional form for the grain size distribution. Although adopting a specific functional form for the grain size distribution is not essential as mentioned below, we explain how to calculate statistical properties.

For convenience, we introduce the ℓ th moment of grain size as

$$\langle a^\ell \rangle_i = \frac{1}{n_{d,i}} \int_0^\infty a^\ell n_i(a) da, \quad (\text{A1})$$

where $n_{d,i}$ is the number density of dust component i (small or large grains) estimated as

$$n_{d,i} = \int_0^\infty n_i(a) da. \quad (\text{A2})$$

The normalization of grain size distribution is written as

$$\frac{4}{3} \pi \langle a^3 \rangle_s n_{d,i} = \mu m_{\text{H}} n_{\text{H}} \mathcal{D}_i, \quad (\text{A3})$$

where s is the material density of dust, n_{H} is the number density of hydrogen nuclei, and m_{H} is the atomic mass of hydrogen. For this normalization, we adopt $s = 3.3 \text{ g cm}^{-3}$

Table A1. Moments.

	$\langle a \rangle$ [μm]	$\langle a^2 \rangle$ [μm^2]	$\langle a^3 \rangle$ [μm^3]	$\langle a^3 \rangle / \langle a^2 \rangle$ [μm]
Small grains	1.2×10^{-3}	2.6×10^{-6}	9.9×10^{-9}	3.8×10^{-3}
Large grains	2.5×10^{-2}	1.1×10^{-3}	8.0×10^{-5}	7.6×10^{-2}

(Draine & Lee 1984) and $\mu = 1.4$. We also need to fix a functional form for $n_i(a)$: we adopt the modified-lognormal form proposed in H15; that is,

$$n_i(a) = \frac{C_i}{a^4} \exp \left\{ -\frac{[\ln(a/a_{0,i})]^2}{2\sigma^2} \right\}, \quad (\text{A4})$$

where we adopt $a_{0,s} = 0.005 \mu\text{m}$, $a_{0,l} = 0.1 \mu\text{m}$ for the central grain radius for small and large grains, respectively, and $\sigma = 0.75$. The assumption on grain size distribution is only for the purpose of calculating quantities that reflects the statistical properties of grain size distribution such as the above moments and extinction curves. We calibrate $a_{0,i}$ and σ so that the Milky Way extinction curve is reproduced with $\mathcal{D}_l = \mathcal{D}_{\text{MW},l} = 0.007$ and $\mathcal{D}_s = \mathcal{D}_{\text{MW},s} = 0.003$. The assumption on the functional form is not essential after such a calibration. For convenience, we list the moments in Table A1. Since the volume-to-surface ratio is important for H_2 formation, we also list $\langle a^3 \rangle / \langle a^2 \rangle$.

APPENDIX B: CALCULATION OF ACCRETION EFFICIENCY β_{ACC}

We summarize the formula for the efficiency of grain growth by accretion (β_{acc}) in H15 (see also Hirashita & Kuo 2011). We refer the interested reader to H15 for the detailed derivation. The accretion time-scale (τ_{acc}) is related to the lifetime of cold cloud (cold clouds mean the gas hosting grain growth by accretion) as $\tau_{\text{acc}} = \tau_{\text{cl}} / (\mathcal{B} X_{\text{cl}})$ where X_{cl} is the cold cloud fraction to the total gas mass, τ_{cl} is the lifetime of the cold clouds, and \mathcal{B} is the increment of dust mass in the cold clouds, which can be estimated as

$$\mathcal{B} \simeq \left[\frac{\langle a^3 \rangle_s}{3y \langle a^2 \rangle_s + 3y^2 \langle a \rangle_s + y^3} + \frac{\mathcal{D}_s}{Z - \mathcal{D}} \right]^{-1}, \quad (\text{B1})$$

where $y \equiv a_0 \xi \tau_{\text{cl}} / \tau$ [a_0 is just used for normalization, $\xi \equiv (Z - \mathcal{D}) / Z$ is the fraction of metals in the gas phase, and τ is the accretion time-scale for a grain with radius a_0], and $\langle a^\ell \rangle_s$ is the ℓ th moment of grain radius for small grains. We adopt the following expression for τ :

$$\tau = 6.3 \times 10^7 \left(\frac{Z}{Z_\odot} \right)^{-1} a_{0.1} n_3^{-1} T_{50}^{-1/2} S_{0.3}^{-1} \text{ yr}, \quad (\text{B2})$$

where $a_{0.1} \equiv a_0 / (0.1 \mu\text{m})$, $n_3 \equiv n_{\text{H}} / (10^3 \text{ cm}^{-3})$ (n_{H} is the number density of hydrogen nuclei in the cold clouds; we adopt $n_{\text{H}} = 10^3 \text{ cm}^{-3}$), $T_{50} \equiv T_{\text{gas}} / (50 \text{ K})$ (T_{gas} is the gas temperature; we adopt $T_{\text{gas}} = 50 \text{ K}$), and $S_{0.3} \equiv S / 0.3$ (S is the sticking probability of the dust-composing material onto the pre-existing grains; we adopt $S = 0.3$). Assuming that the cold clouds hosting accretion and star formation are the same, we can express the star formation time-scale as $\tau_{\text{SF}} = \tau_{\text{cl}} / (\mathcal{E} X_{\text{cl}})$,

where ε is the star formation efficiency of the cold clouds. We define $\beta_{\text{acc}} \equiv \tau_{\text{SF}}/\tau_{\text{acc}}$, which can be evaluated as

$$\beta_{\text{acc}} = \frac{\mathcal{B}}{\varepsilon}. \quad (\text{B3})$$

We assume $\varepsilon = 0.1$ in this paper.

This paper has been typeset from a $\text{T}_{\text{E}}\text{X}/\text{L}^{\text{A}}\text{T}_{\text{E}}\text{X}$ file prepared by the author.